Pyrophoric Ignition System Development for Hybrid Rocket Motors in Space Applications

by

Miray Karpat

A Dissertation Submitted to the
Graduate School of Sciences and Engineering
in Partial Fulfillment of the Requirements for
the Degree of

Master of Science

in

Mechanical Engineering

KOÇ
ÜNİVERSİTESİ

January 5, 2023

Pyrophoric Ignition System Development for Hybrid Rocket Motors in Space Applications

Koç University

Graduate School of Sciences and Engineering

This is to certify that I have examined this copy of a master's thesis by

Miray Karpat

and have found that it is complete and satisfactory in all respects,
and that any and all revisions required by the final
examining committee have been made.

Committee Members:

Assoc. Prof. Dr. Arif Karabeyoğlu

Prof. Dr. Metin Muradoğlu

Prof. Dr. Onur Tunçer

Date: January 5, 2024

To my family…

ABSTRACT

Pyrophoric Ignition System Development for Hybrid Rocket Motors in Space Applications

Miray Karpat

Master of Science in Mechanical Engineering

January 5, 2024

Hybrid motors are gaining attention in space applications due to their advantageous features like inherent safety and controllability, standing out against conventional solid and liquid engines. However, achieving rapid and reliable ignition remains a significant challenge for hybrid motors, particularly for their use in space systems. Among the various ignition methods, pyrophorics show promising characteristics. In this thesis, ignition delay characteristics of a pyrophoric liquid triethylaluminum (TEA) with nitrous oxide (N_2O), a commonly employed self-pressurizing oxidizer, has been investigated for impinging jets, and the feasibility for an ignition system has been evaluated. A series of experiments were conducted to determine ignition delay values and ignition boundaries for two different oxidizer-to-fuel (O/F) ratios by changing the impingement angle. Results have demonstrated relatively favourable TEA/N_2O ignition delays across varying impingement angles. This research also comprehensively evaluates experimental outcomes, post-test equipment conditions along with the theoretical aspects to outline the design criteria for a comprehensive ignition system.

ÖZETÇE

Uzay Uygulamalarında Hibrit Roket Motorları için Piroforik Ateşleme Sistemi Geliştirilmesi

Miray Karpat

Makine Mühendisliği, Yüksek Lisans

5 Ocak 2024

Hibrit motorlar, geleneksel katı ve sıvı motorlara göre öne çıkan, özünde olduğu şekilde emniyet ve kontrol edilebilirlik gibi avantajlı özellikleri nedeniyle uzay uygulamalarında dikkat çekmektedir. Ancak hızlı ve güvenilir ateşlemenin sağlanması, hibrit motorlar ve özellikle uzay sistemlerindeki kullanımları için önemli bir zorluk olmaya devam etmektedir. Çeşitli ateşleme yöntemleri arasında piroforikler umut verici özellikler göstermektedir. Bu tezde, yaygın olarak kullanılan ve kendi kendini basınçlandırma özelliği gösteren bir oksitleyici olan nitröz oksit (N_2O) ile birlikte piroforik sıvı trietilalüminyumun (TEA) ateşleme gecikmesi özellikleri, çarpan jetler için araştırılmış ve bir ateşleme sistemi için fizibilitesi değerlendirilmiştir. Çarpma açısını değiştirerek iki farklı oksitleyici-yakıt (O/F) oranı için ateşleme gecikmesi değerlerini ve ateşleme sınırlarını belirlemek amacıyla bir dizi deney yapılmıştır. Sonuçlar, farklı çarpma açıları için nispeten tercih edilir TEA/N_2O ateşleme gecikmeleri göstermiştir. Bu araştırmada aynı zamanda, kapsamlı bir ateşleme sistemi için tasarım kriterlerinin ana hatlarını çizmek amacıyla deneysel sonuçlar, test sonrası ekipmanların durumları ve teorik yönler kapsamlı bir şekilde değerlendirilmektedir.

AKNOWLEDGEMENTS

Firstly, I extend my sincere gratitude to my advisor, Assoc. Prof. Arif Karabeyoğlu. His guidance, expertise, and continuous support have been important throughout this research journey. His insightful advice and continuous encouragement have significantly shaped and strengthened this work. It is a privilege working with him, and I feel lucky for having him as my advisor.

Additionally, I would like to express my appreciation to my jury members Prof. Dr. Onur Tunçer and Prof. Dr. Metin Muradoğlu for their thorough review and valuable comments.

I also would like to thank DeltaV Space Technologies Inc. for providing test facilities, materials, and manufacturing support. These resources were crucial for conducting experiments and acquiring necessary materials for this research.

I would like to especially thank Fatih Emin Satikbuğa for his unlimited and unconditional support. His thoughts and guidance have always been invaluable, helping me overcome critical milestones of this research. Moreover, I am thankful for his remarkable courage in facing the challenging and hazardous aspects of this study. He is, and always will be, my favourite colleague and dearest friend. I am forever grateful.

I want to extend my heartfelt thanks to my dogs, Hera and Kahve, for being in my life. Their companionship and comforting presence have been my emotional rock. Their wagging tails and unconditional love have brought joy to my life during these challenging times.

Lastly, but most importantly, I want to express my deepest gratitude to my mother, Yıldız Karpat, my father, Bülent Karpat and my brother, Onur Karpat for their unconditional love and support, encouragement and understanding. I am forever grateful to my parents for the efforts they made in raising me; their support has meant everything to me.

TABLE OF CONTENTS

List of Tables ix

List of Figures x

Nomenclature xii

Chapter 1: Introduction 1

1.1 Motivation 1

1.2 Rocket Propulsion Systems 1

1.2.1 Solid Motors 2

1.2.2 Liquid Engines 2

1.2.3 Hybrid Motors 3

1.3 Ignition Systems 4

1.3.1 Spark Ignition 5

1.3.2 Augmented Spark (Torch) Ignition 6

1.3.3 Pyrotechnics 7

1.3.4 Catalyzed Ignition 8

1.3.5 Plasma Torch Ignition 9

1.3.6 Combustion Wave Ignition 9

1.3.7 Resonance Ignition 10

1.3.8 Hypergolic Ignition 10

1.4 Literature Review 12

1.5 Objectives and Outline of the Thesis 16

Chapter 2: Triethylaluminum 17

2.1 Physical and Chemical Properties 18

2.2 Safety and Handling 20

2.2.1 General Safety Measures and Equipment Preparations 20

2.2.2 Transfer and Quenching/Cleaning Procedures 22

2.2.3 Potential Hazards 24

2.3 Reaction with Nitrous Oxide 26
2.3.1 Stoichiometric O/F Ratio 27
2.3.2 Performance Parameters 27
2.3.3 Comparison with Various Igniters 30
Chapter 3: Experimental Evaluation 34
3.1 Design 34
3.1.1 TEA Injector 34
3.1.2 N_2O Injector 34
3.1.3 TEA Tank 36
3.2 Experimental Setup 37
3.3 Test Campaign 40
3.3.1 Ignition Delay and Boundary Determination 40
3.3.2 Mixed Spray Temperature Measurement 43
3.3.3 Data Analysis 44
Chapter 4: Results and Discussion 46
4.1 Ignition Delay and Boundary Determination Results 46
4.2 Mixed Spray Temperature Measurement Results 48
4.3 Discussion 49
4.3.1 Reactive Stream Separation 49
4.3.2 Post-test Status of the Materials 52
Chapter 5: Conclusion 54
Bibliography 56

LIST OF TABLES

Table 2.1: Physical and chemical properties of TEA. 19
Table 2.2: Risk assessment. 24
Table 2.3: Properties of N_2O. 26
Table 2.4: Maximum T_c and c* with corresponding O/F ratios for different chamber pressures. 30
Table 2.5: Maximum T_c and c* with corresponding O/F ratios for different propellant pairs. 33
Table 3.1: Test parameters. 40
Table 3.2: Test matrix. 41
Table 4.1: Summary of test results. 47

LIST OF FIGURES

Figure 1.1: Small hybrid motors used as igniters (adapted from [8]). 6
Figure 1.2: Augmented spark igniter (adapted from [11]). 7
Figure 1.3: Pyrogen ignition system (adapted from [12]). 8
Figure 1.4: Combustion wave ignition system (adapted from [11]). 10
Figure 1.5: Resonance igniter (adapted from [11]). 11
Figure 1.6: 250-klbf motor liquid-oxygen injector design (adapted from [31]). 13
Figure 1.7: AMROC motor configuration; 26-LOX injector, 32-LOX spray, 34-ignition fluid injector, 36-ignition fluid spray (adapted from [32]). 15
Figure 1.8: Aftport pressure profiles of three short firings (adapted from [32]). 15
Figure 1.9: Aftport pressure of a 70-second-duration motor firing with continuous TEA injection (adapted from [32]). 16
Figure 2.1: Molecular structure of TEA dimer. 19
Figure 2.2: Glovebox system. 23
Figure 2.3: Transfer procedure. 23
Figure 2.4: Chemical baths used for quenching. 24
Figure 2.5: Variation of T_c and c* for pressure values (a) P_c = 1 bar, (b) Pc = 10 bar, (c) Pc = 20 bar, (d) Pc = 30 bar. 29
Figure 2.6: Variation of T_c and c* at P_c = 20 bar for (a) Paraffin/N_2O, (b) HDPE/N_2O, (c) PA6-6/N_2O, and (d) Al+Paraffin/N_2O. 32
Figure 3.1: TEA injector. 35
Figure 3.2: N_2O injector 35
Figure 3.3: TEA tank. 36
Figure 3.4: Test setup P&ID. 38
Figure 3.5: Experimental setup. 39
Figure 3.6: 3D model of 60° bracket (a) isometric view, (b) side view. 42
Figure 3.7: 60° ignition test with O/F ratio of 2.76. 42
Figure 3.8: Spray temperature measurement setup. 43
Figure 3.9: The ignition test for spray temperature measurement. 44
Figure 4.1: Variation of ignition delay times with respect to impingement angle for (a) O/F ratio of 2.7 and (b) O/F ratio of 4.3. 47
Figure 4.2: Mixed spray temperature measurements. 49

Figure 4.3: Impinging hypergolic streams in the case of (a) mixing and (b) separation (adapted from [48]). 50
Figure 4.4: Post-test Al_2O_3 accumulation. 52
Figure 4.5: Fitting deformation due to leakage. 53

NOMENCLATURE

A_c	Orifice area
Al	Aluminum
Al_2O_3	Aluminum oxide
AV	Automatic valve
c*	Characteristic velocity
CAD	Computer aided drafting
C_d	Discharge coefficient
D	Orifice diameter
DAQ	Data acquisition system
EPDM	Ethylene propylene diene monomer
FFKM	Perfluoroelastomer
FKM	Fluoroelastomers
GOX	Gaseous oxygen
HDPE	High-density polyethylene
HTPB	Hydroxyl-terminated polybutadiene
I_{sp}	Specific impulse
LOX	Liquid oxygen
$\dot{m}$	Mass flow rate
MEOP	Maximum expected operating procedure
MV	Manual valve
N_2	Nitrogen
N_2O	Nitrous oxide
NBR	Nitrile butadiene rubber
O/F	Oxidizer-to-fuel
P&ID	Piping and instrumentation diagram
PA6-6	Polyamide 6-6
P_c	Chamber pressure
PPE	Personal protective equipment
PT	Pressure transducer
PTFE	Polytetrafluoroethylene
SF	Safety factor
SOP	Standard operating procedure
T_c	Chamber temperature
TC	Thermocouple
TPE	Thermoplastic elastomer
TPV	Thermoplastic vulcanizates
V	Jet velocity

Greek Symbols

θ	Impingement angle
ρ	Density
τ_{ign}	Chemical reaction time
τ_{mix}	Mixing time
ΔP	Pressure drop

Chapter 1:
INTRODUCTION

1.1 Motivation

Hybrid rocket propulsion systems represent a critical advancement in space propulsion technology, combining the advantages of solid and liquid propulsion systems. These systems utilize the combination of solid fuel grains and liquid/gaseous oxidizers. Their significance lies in their enhanced safety and controllability such as shut down, restart and throttling. At this point, the ignition system becomes quite crucial, enabling reliable multiple ignitions. An igniter provides the necessary heat to for the ignition of propellants. Selection of the ignition method poses a significant challenge and depends on various attributes such as propellants, safety, reliability, and restart capabilities. For a space propulsion system, multiple ignitions with high reliability are as critical as system safety. At this point, development of an ignition system that operates with high degree of reliability and restart capability becomes essential. The use of pyrophoric reagents holds promise in delivering these essential attributes.

Pyrophoric ignition involves the spontaneous and rapid ignition of pyrophoric materials upon exposure to air or oxidizers, contributing to the overall system reliability. This study will mainly focus on the ignition capability and performance of a pyrophoric liquid, namely triethylaluminum, combined with nitrous oxide as oxidizer intended for used as an ignition source.

1.2 Rocket Propulsion Systems

Propulsion denotes the alteration of an object's motion. Rocket propulsion systems are categorized according to their energy sources: namely, chemical, nuclear, or electric. Within chemical rockets, an exothermic chemical reaction occurs within the combustion chamber, producing high-pressure, heated combustion gases. These gases are then expanded through a nozzle, converting thermal energy into high-velocity exhaust crucial for generating thrust. Chemical rocket engines are further classified based on the storage phase of propellants, distinguishing into solid motors, liquid engines, and hybrid motors.

1.2.1 Solid Motors

Solid motors are designed with oxidizer and fuel stored within a premixed solid grain confined within the combustion chamber. Their mechanical simplicity distinguishes them from other propulsion systems, as they do not require external propellant tanks, fluid handling valves, injectors, or pressurization systems. When optimized, solid motors exhibit a specific impulse (I_{sp}) reaching up to 290s [1]. They are highly favored in missile applications due to their ability to deliver substantial thrust within a compact structure.

These motors find extensive use as side or main stage boosters in launch vehicles, as well as in escape systems and apogee kick motors. However, their ability to be stored for extended periods in both ground-based and vacuum environments, solid fuel grains exhibit inherent hazards due to the premixed nature of oxidizer and fuel elements. Consequently, careful handling becomes critical during transportation, storage, and application, inevitably leading to escalated developmental and operational costs. Their capacity for long-term storage, both in ground applications and vacuum environments, notwithstanding, solid fuel grains pose significant safety concerns.

A notable limitation of solid motors lies in their inability to be actively shut down or throttled during flight, restricting their operational flexibility. Moreover, their single-use nature rules out any possibility of reusability. This constraint marks a substantial disadvantage in comparison to other propulsion systems that offer reusability options. As a result, the single-use attribute of solid motors necessitates their careful consideration in mission planning and execution.

1.2.2 Liquid Engines

Liquid engines are more complex compared to other engine types, given their inclusion of various elements like valves, injectors, turbopumps, and propellant tanks. Their primary advantages lie in their high performance, controllability, and potential for reuse. These engines enable restarts, shutdowns, and throttling as they regulate liquid propellants through valves. Typically achieving an I_{sp} performance of approximately 310 s, some engines even reach up to 420 s in this metric [1] [2]. However, a drawback of liquid engines stems from their heightened performance, which leads to increased intricacy, subsequently elevating development costs.

Liquid engines are commonly classified as monopropellants and bipropellants. In bipropellant engines, the oxidizer and fuel are stored separately and mixed within combustion chambers during operation. While many propellant combinations require an external heat source for ignition, hypergolics initiate combustion upon contact, although they pose explosion hazards and often are toxic, carcinogenic, and corrosive [3]. Cryogenic propellants, which liquefy at temperatures significantly lower than the ambient temperature, offer relatively high performance but lack long-term storability. Conversely, storable propellants remain stable across a reasonable range of temperature and pressure values, allowing for extended storage in sealed tanks.

Monopropellant engines, unlike bipropellants, utilize a single substance as both the fuel and oxidizer, decomposed by a heated catalyst. This process generates hot gases through an exothermic reaction, expelled through a nozzle to create thrust. Commonly employed monopropellants include hydrazine and hydrogen peroxide. Commonly employed monopropellants include hydrazine and hydrogen peroxide. These engines boast a simpler design and operation compared to bipropellants, relying on a single propellant. However, they offer a moderate I_{sp}, averaging around 230 s [1]. They are usually utilized in small spacecraft like thrusters, satellites, and space probes.

1.2.3 Hybrid Motors

Hybrid motors utilize a combination of solid fuel and liquid oxidizer as their propellants. Typically, in these rocket motors, the solid fuel is housed within the combustion chamber, while the oxidizer is stored in an external tank. The primary components of a hybrid motor encompass pressurant and oxidizer tanks, fluid valves, injectors, and the thrust chamber. When dealing with low-pressure oxidizers, a pressurization system becomes necessary to propel the oxidizer into the combustion chamber, which may involve pumps or a separate tank containing pressurant gas. In comparison to liquid engines, hybrid motors exhibit reduced complexity due to the management of a single fluid system, resulting in fewer valves, feed line instruments, and tanks. This feature contributes to decreased developmental and operational expenses. The thrust chamber comprises various elements including the injector, igniter, pre-combustion chamber, solid fuel grain, post-combustion chamber, and nozzle. An igniter element initiates the preheating of the combustion chamber before the oxidizer's flow. The energy

released by the igniter pyrolyzes the solid fuel, which subsequently undergoes combustion upon contact with the liquid oxidizer's resulting gaseous pyrolysis products.

Unlike solid motors, hybrid motors offer the capability for shut down, restart, and throttling. An experimental investigation conducted by Whitmore, Peterson, and Eilers showcased a series of successful tests involving the throttling of hybrid [4] [5]. Additionally, these motors demonstrate higher resilience to pressure fluctuations, variations in propellant temperature, debonding, and cracks in comparison to solid motors. The primary advantage of hybrid motors lies in their inherent safety. In hybrids, the fuel and oxidizer are stored separately in distinct phases, eliminating pre-mixing. Since an external heat source is necessary to initiate combustion, the risk of an explosive event due to the mixing of oxidizer and fuel is eliminated.

One drawback of hybrid motors lies in their lower regression rates, making it challenging to achieve higher thrust levels. Enhancing regression rates can be achieved through methods like using longer grains or incorporating multiple grain ports of different shapes to increase the burning surface area. However, there are several manufacturing challenges associated with multiple port grains. Research conducted by the Space Propulsion Group suggests that employing high regression fuel formulations and innovative oxidizers presents potential solutions to this challenge [6]. Hybrid motors also experience O/F (oxidizer-to-fuel) shift during the burning process. Contrary to common idea, the variation in O/F is not as significant as commonly assumed [7].

A wide array of fuel-oxidizer combinations exists for hybrid rocket motors, commonly employing solid fuels like hydroxyl-terminated polybutadiene (HTPB) and hydrocarbon-based paraffin wax. These fuels are typically coupled with liquid oxygen (LOX), nitrous oxide (N_2O), or occasionally, gaseous oxygen (GOX). Most of these propellant combinations are readily accessible in industrial settings, known for their non-toxic nature and safer handling, contributing to reduced development expenses and increased safety standards.

1.3 Ignition Systems

The majority of propellant combinations do not spontaneously react upon contact, unlike hypergolics. Hence, an external heat source is essential to initiate the combustion process. An ignition system facilitates the required heat release for propellant reaction,

typically not needing continuous maintenance throughout engine operation. Once the primary propellants are ignited, the combustion process becomes self-sustaining, eliminating the necessity for a continual ignition source.

Ignition stands as a pivotal challenge in chemical propulsion systems, with the selection of an appropriate method depending on numerous factors. These include the propulsion system type, propellant phase and properties, alignment with system design, overall weight and complexity considerations, safety, reliability, and restart needs. To avoid catastrophic hard starts in systems using mono-propellant or bi-propellant liquids, ensuring a smooth ignition sequence is particularly vital. Additionally, in systems employing multiple engines or staging, precise ignition timing is crucial to prevent asymmetric thrust distribution resulting from any ignition delays. Vehicle and propulsion system design heavily influence the choice of ignition method, with a strong preference for reduced complexity and minimal dry mass, often favoring systems that utilize existing propellants. This approach is typically more feasible in liquid propulsion systems but less so in hybrid motors. However, in all cases, the primary emphasis is on achieving rapid and reliable ignition. Delayed ignition can lead to the accumulation of unignited propellants, potentially forming reactive mixtures and risking combustion chamber explosions. Consequently, minimizing ignition delay time becomes a critical igniter design parameter to avert such situations, highlighting the importance of a well-chosen ignition system.

There exist numerous ignition systems employing hypergolic or pyrophoric reactants, spark plugs, augmented high voltage sparks (referred to as liquid bi-propellant torches), pyrotechnics, catalyzed monopropellants, and high-power plasma arcs. Another commonly employed ignition approach in hybrid rocket propulsion involves utilizing a small-scale hybrid motor to ignite a larger one, as depicted in Figure 1.1 [8]. This research will primarily focus on the pyrophoric ignition method and its associated system development.

1.3.1 Spark Ignition

This ignition method involves a small device known as a spark plug, positioned within the combustion chamber. This plug connects to a high voltage source generated by a coil. When the current passes through, it generates a voltage difference between the

electrodes. This produces an arc between the electrodes, generating intense heat that elevates the propellants' temperature, initiating ignition. While spark plugs find extensive use in internal combustion engines, they're also utilized in various forms for liquid propellant rocket engines [2]. However, their historical use in hybrid rocket motors remains relatively limited.

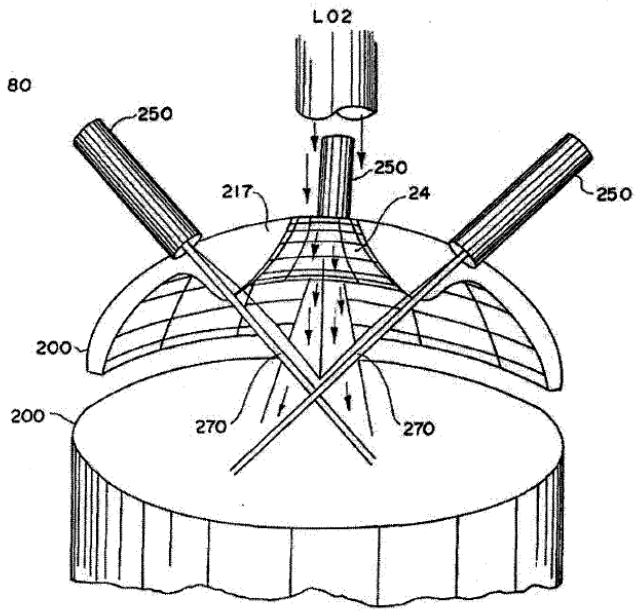

Figure 1.1: Small hybrid motors used as igniters (adapted from [8]).

1.3.2 Augmented Spark (Torch) Ignition

Augmented spark igniters, often referred to as bi-propellant torch igniters, function as miniature liquid bi-propellant rocket engines with significantly lower flow rates, typically ranging between 0.1-0.3% of the main propellant mass flow rates. These igniters instigate reactant mixture using a spark plug positioned within a separate, relatively compact igniter combustion chamber. The resulting combustion flame is directed into the engine's primary combustion chamber, generating the necessary heat for igniting the main propellants. Notably, these igniters commonly employ the main propellants as reactants to eliminate the need for additional propellants and feed system instruments. A basic design of an augmented spark igniter is given in Figure 1.2.

Augmented spark igniters offer several advantages in terms of durability, system performance, and reduced complexity. They exhibit reusability across a wide range of mass flow rate values and O/F ratios. Additionally, their extended lifespan and capability to operate in demanding environments position them as excellent choices for in-space

applications. They have demonstrated successful utilization in various systems, including the Space Shuttle's main engine, J2 liquid engines, and the Vinci upper stage engine [2] [9] [10].

Despite their high reliability, augmented spark igniters share drawbacks similar to those of liquid bi-propellant engines, such as the potential for hard starts and increased complexity. While their advantage of utilizing main propellants for ignition eliminates the need for additional ignition chemicals, this advantage is somewhat restricted in hybrid motor applications due to the effective utilization of only one of the propellants.

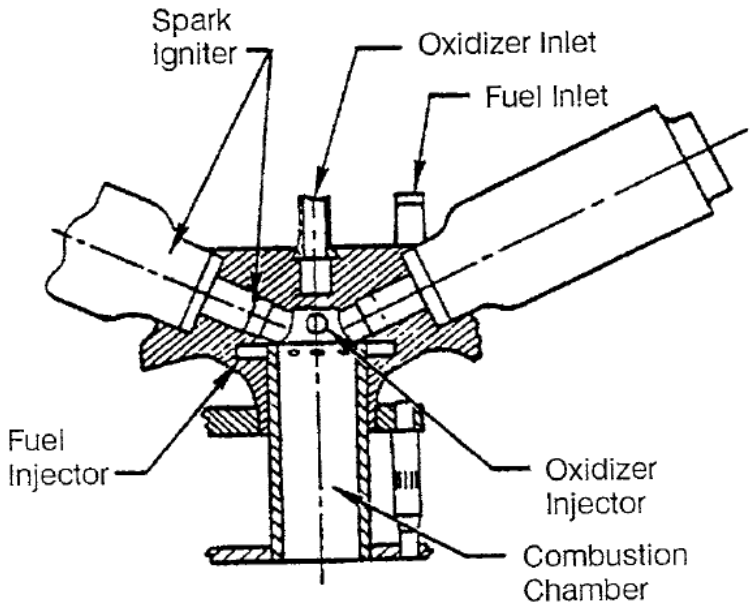

Figure 1.2: Augmented spark igniter (adapted from [11]).

1.3.3 Pyrotechnics

Pyrotechnic igniters function as compact solid motors containing pre-mixed solid oxidizer and fuel combinations, housing a resistive bridge wire within, as shown in Figure 1.3. Upon the passage of electrical current through this wire, the heat-sensitive solid grain ignites, producing a high-temperature sheet of flame. Directed into the main engine's combustion chamber, this flame supplies the necessary heat to ignite the main propellants.

Widely utilized in solid and hybrid rocket motors [12], pyrotechnic igniters offer reliability and reduced system complexity owing to their primitive design. However, their single-use nature prevents restarts and exposes them to similar disadvantages and risks associated with solid motors. Consequently, they require special and careful handling, which unfortunately compromises the inherent safety attributed to hybrid rockets.

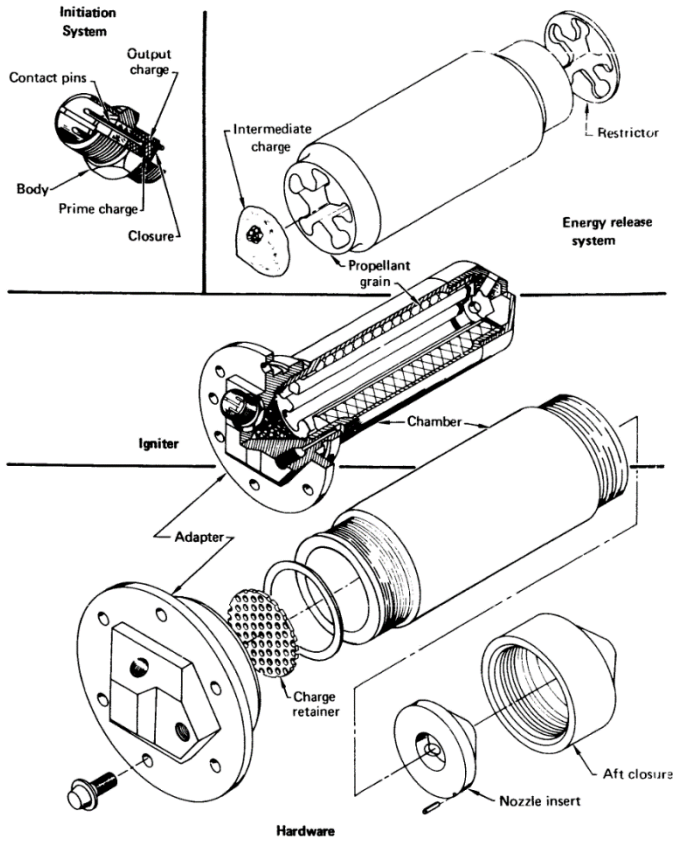

Figure 1.3: Pyrogen ignition system (adapted from [12]).

1.3.4 Catalyzed Ignition

Catalytic ignition occurs as a propellant passes through a catalyst bed, generating hot combustion gases directed into the combustion chamber to initiate the main propellants. Hydrazine and hydrogen peroxide (H_2O_2) are the most commonly catalytically ignited propellants, with hydrogen peroxide extensively studied for its compatibility with various catalyst beds. In the recent years, there is an increased and renewed interest in the use of H_2O_2 as an oxidizer for hybrid propulsion systems [13] [14].

Numerous research endeavors are underway concerning the catalytic decomposition of nitrous oxide [15] [16]. Given its widespread use as an oxidizer in hybrid rockets, the catalytic decomposition of nitrous oxide arises as a promising ignition method. However, several technical obstacles must be addressed when establishing a reliable system. One such challenge involves the inclusion of additional components to provide substantial power and current for heating the catalyst bed to the requisite level for nitrous oxide decomposition. Moreover, ensuring the integrity and effectiveness of the catalyst during operation presents another critical obstacle.

1.3.5 Plasma Torch Ignition

In a plasma torch igniter, electrical energy is employed to elevate the temperature of a gas, creating a high-temperature plasma flow directed into the combustion chamber. This flowing gas, which may constitute one of the propellants like hydrogen or methane, reduces the necessity for additional reactants. However, the primary drawback of such systems is the substantial requirement for high electrical power input. As the gas heating relies solely on electrical energy without any support from chemical reactions, significant levels of current and power are essential. Various research studies have investigated plasma arc igniters, not only for rocket engines but also for air-breathing engines [17] [18].

1.3.6 Combustion Wave Ignition

In engines designed with segmented configurations and injectors featuring multiple partitions, igniting at a single location is often impractical. Employing more than one single-point ignition source increases both the complexity and cost of the system. However, a simpler approach involves utilizing a single, compact igniter with branched outputs to achieve multipoint ignition. This design concept is known as combustion-wave igniters.

The setup, as given in Figure 1.4, comprises a precombustor, sparkplug, branched manifold, pilot flow injectors, and associated propellant feed components like control valves. Pilot flow injection elements are mounted on the main propellant injector plate at specified locations. Propellants are directed into the igniter precombuster while initiating the spark plug. Simultaneously, pilot flow valves are activated. Once combustion initiates, the resulting flame or deflagration wave progresses with the flow. Eventually, a detonation wave forms and spreads through the branches, igniting the pilot flow of propellants. The ensuing pilot flames then ignite the main propellants at desired locations. However, this system's drawback lies in the increased hardware requirements, significantly elevating complexity and overall system weight. Several experimental studies have explored combustion wave ignition systems [19] [20].

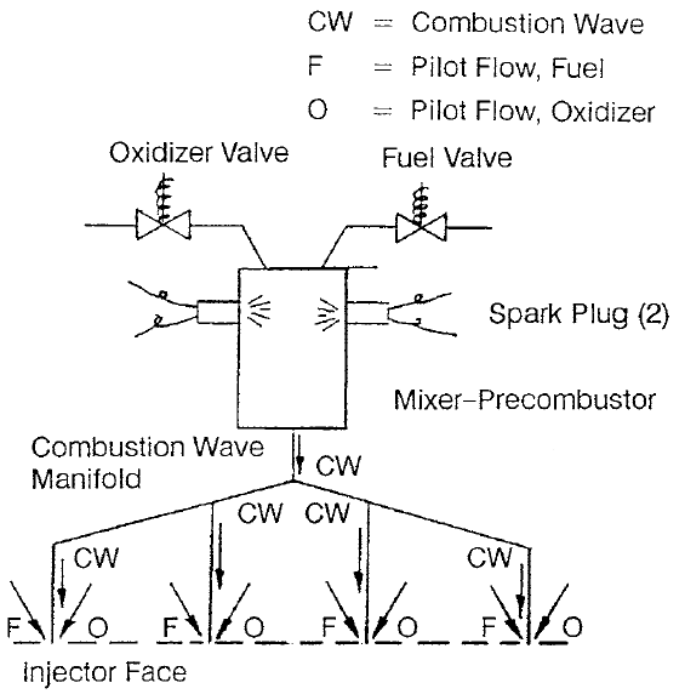

Figure 1.4: Combustion wave ignition system (adapted from [11]).

1.3.7 Resonance Ignition

The schematic of a resonance igniter is depicted in Figure 1.5. In this setup, pressurized gaseous propellants undergo ignition through resonance heating. Initially, high-pressure gas, like hydrogen, enters the sonic nozzle, expands into the mixing chamber. Then, it proceeds into the resonance cavity where it undergoes cyclical compression and expansion. As the gas attains the necessary temperature, oxidizer, such as oxygen, is introduced into the heated fuel gas, aiding in ignition. The primary advantage of this method lies in its independence from electrical power, moving components, or catalysts. Both numerical simulations and experimental investigations have been conducted on resonance igniters [21] [22].

1.3.8 Hypergolic Ignition

Hypergolic igniters rely on hypergolic reactants that spontaneously ignite upon contact. Hypergolic combinations can serve as the ignition system alone or act as the primary propellant for the engine. Notable examples of engines utilizing hypergolic ignition encompasses the Rocketdyne F1 used in the Saturn V vehicle and the SpaceX Merlin engine series [23] [24]. In instances where hypergols are used as the ignition

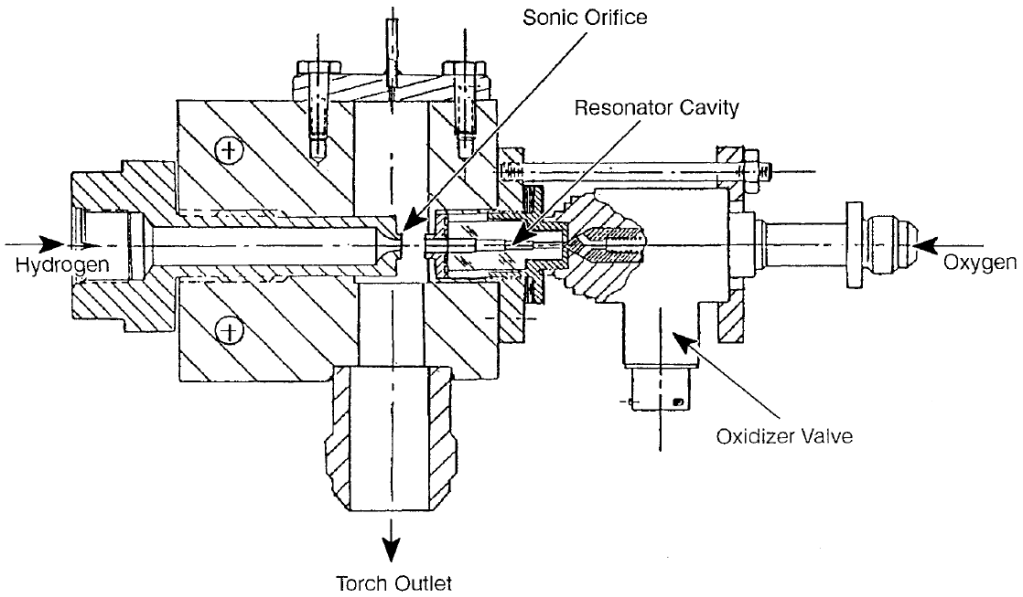

Figure 1.5: Resonance igniter (adapted from [11]).

system for non-hypergolic main propellants, a 'plug' of hypergolic or pyrophoric liquid leads the main propellant flow, igniting the chamber. This approach simplifies the ignition system by eliminating the need for precise timing coordination between main propellant valves and igniter events.

When at least one of the main propellants is used as an igniter reactant alongside hypergols, bipropellant systems can employ hypergolic ignition without requiring an additional self-contained fluid system. However, solid and hybrid motors necessitate a separate igniter fluid system to maintain the separation of igniter reactants. Commonly used hypergolic propellant combinations include monomethyl hydrazine, hydrazine, and unsymmetric dimethylhydrazine paired with nitrogen tetroxide or nitric acid.

Pyrophoric reactants are part of the hypergolic family and ignite spontaneously upon contact with air and/or water. Among the commonly used pyrophoric liquids for ignition sources is the TEA-TEB pair, for example employed in Falcon 9 Merlin engines as a dual redundant igniter [24].

Hypergolic systems offer the benefit of delivering a straightforward and exceptionally reliable ignition process. However, their elevated reactivity makes hypergolic and pyrophoric liquids highly toxic and/or carcinogenic. Furthermore, in cases where systems necessitate restart capability, the management and delivery of igniter reactants demand additional tanks, feedlines, and valves. Nonetheless, hypergolic and/or

pyrophoric reactants remain a preferred ignition source for critical ignition events, particularly in space-oriented applications.

1.4 Literature Review

In a pyrophoric ignition system, the pyrophoric liquid is used with at least one of the propellants in a bi-propellant liquid rocket engine. In the case of hybrid motors, the pyrophoric liquid is generally used with the oxidizer without introducing any additional ignition reactant. Due to their pyrophoric nature, these liquids ignite upon contact with air, even without the presence of the oxidizer, thus increasing the reliability and efficiency, and decreasing system complexity.

In the literature, numerous studies on hybrid rocket motors have utilized different pyrophorics as ignition sources. In the late 80s and early 90s, American Rocket Company (AMROC) used triethylaluminum (TEA) to ignite their liquid oxygen/polybutadiene hybrid motors [25] [26] [27] [28]. The design was such that TEA is injected coaxially with LOX into the combustion chamber, and occurred reaction vaporizes the fuel on the grain surface forming a layer of fuel. Helium was used to pressurize the TEA tank. It is also reported that the motor ignitions were smooth, and no overshoot was observed in the chamber pressure [28].

Another hybrid motors utilizing pyrophorics as ignition sources were developed by The Hybrid Propulsion Demonstration Program (HPDP). The program started in 1995 and participants included NASA, DARPA, Lockheed Martin, United Technologies Chemical Systems Division, Thiokol, Rocketdyne, Allied Signal, and Environmental Aeroscience. Several 11-inch and 24-inch subscale motors was tested for understanding of large-scale hybrid rocket propulsion systems [29]. These LOX fed subscale motors were ignited using a 15%/85% mixture of triethylaluminum and triethylborane (TEA/TEB). The pyrophoric mixture was injected into the combustion chamber, thus providing the necessary ignition source for the oxidizer by reacting with the ambient air inside the motor. HPDP also conducted a stability analysis on 11-inch motors using LOX [30]. Each motor was ignited by the 85/15 mixture of TEA/TEB. The sequence of the valves was such that the TEA/TEB flow leads the LOX arrival by approximately 150 ms ahead. TEA/TEB flowed approximately 1.5 s with a rate of 0.2 lb/s (90.7 g/s). Ignition of the motor and the establishment of main-stage conditions were approximately 500 ms. It

is reported that the effect of TEA/TEB combustion on stability appears to be significant in some cases, while in others, it is less pronounced, based on the examination of motor pressure data. In one of the tests, pressure oscillations seemed to be grown after the TEA/TEB flow was terminated. Some other tests exhibited a momentary chamber pressure drop after the TEA/TEB was cut, yet no major change was observed in combustion characteristics. In some tests, no effect was noticed. It was concluded that, overall, introducing TEA/TEB during the main-stage operation had little impact on enhancing combustion stability.

Based on the 24-inch subscale tests mentioned earlier, HPDP designed a 250-klbf thrust, 73-inch motor utilizing liquid oxygen/hydroxyl terminated polybutadiene /polycyclopentadiene (LOX/HTPB/PCPD). Among the two motor design concepts considered, one used a pyrophoric ignition system. TEA/TEB mixture was supplied through three equally spaced, 0.375 in. diameter orifices drilled in the main injector body, as shown in Figure 1.6. The flow rate of TEA/TEB is 3 lbm/sec for a duration of 5 sec [31].

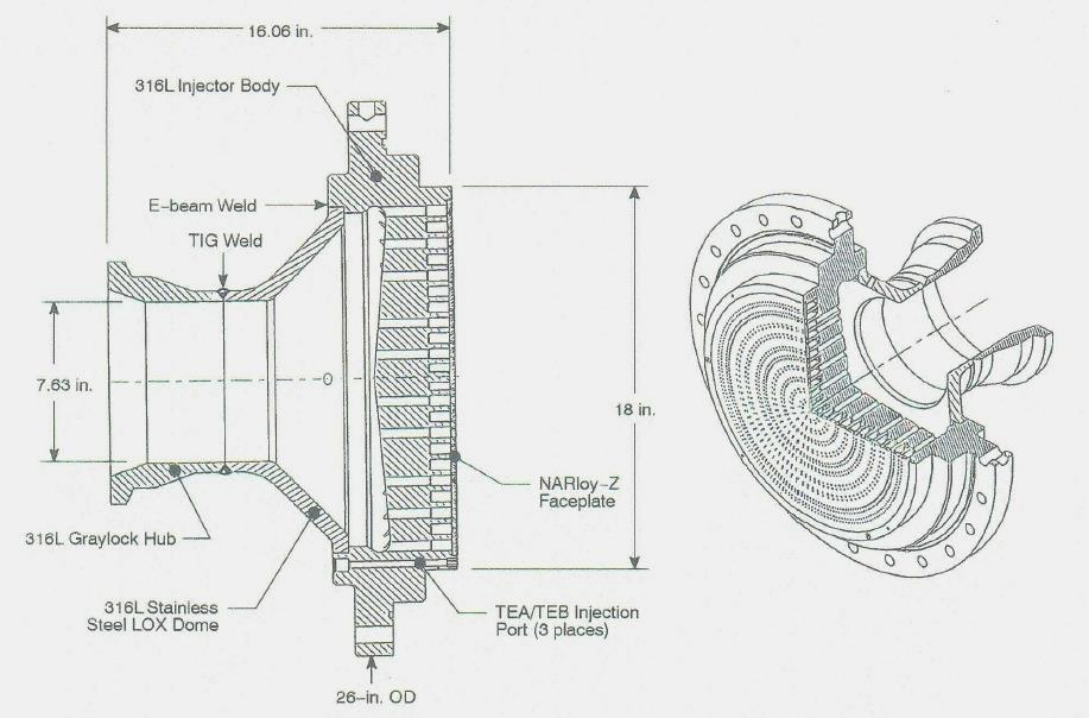

Figure 1.6: 250-klbf motor liquid-oxygen injector design (adapted from [31]).

Other than ignition purposes, TEA was used to eliminate low frequency instabilities. According to the claims in AMROC's patent, by continuously injecting a pyrophoric fluid into the combustion chamber all the liquid oxidizer is vaporized before entering the combustion zone which in turn eliminates the boundary layer problem causing the low frequency instabilities. Erratic combustion may occur due to unvaporized liquid oxidizer flow, disrupting the stable boundary layer combustion process. In an ideal combustion scenario, a combustion zone is established within the boundary layer where vaporized fuel and oxidizer meet, providing the necessary heat for fuel vaporization. However, when unvaporized liquid oxidizer spreads across the surface of the solid grain, it reduces the temperature of the forward reaction mixture, causing the efficient combustion to shift towards the aft section of the motor. As the pressure differences grow in the combustion area, hot reaction products move back and forth, creating low-frequency oscillations along the length of the grain, leading to unsteady combustion and unstable thrust distribution [32].

To solve this problem, AMROC suggested that injecting pyrophoric fluid into the oxidizer stream can vaporize the entire liquid oxygen before entering the combustion zone. It is stated that for a hybrid motor utilizing LOX as oxidizer and TEA as pyrophoric fluid, complete vaporization of the oxidizer can be achieved by setting the pyrophoric liquid flow rate at approximately 0.1% of the weight of the liquid oxidizer. However, flow rates exceeding 5% of the oxidizer's weight are excessive and may result in unstable combustion [32]. They also provided test data from four different motor firings using the configuration given in Figure 1.7 to support their claim. In Figure 1.8, aft port pressure profiles of three short firings were compared. H8#1 utilized TEA only during the initial startup period of the motor, whereas H8#2 and H8#3 motors were operated with a continuous injection of TEA. All three motors operated under the identical conditions. It can be seen from Figure 1.8 that while H8#1 exhibits low frequency instabilities, H8#2 and H8#3 shows no low frequency harmonics. Another example test provided by AMROC is given in Figure 1.9, which has a long burn time of 70 seconds with continuous TEA injection. It is reported that the aft port pressure is steady during the combustion with no low frequency instabilities [32].

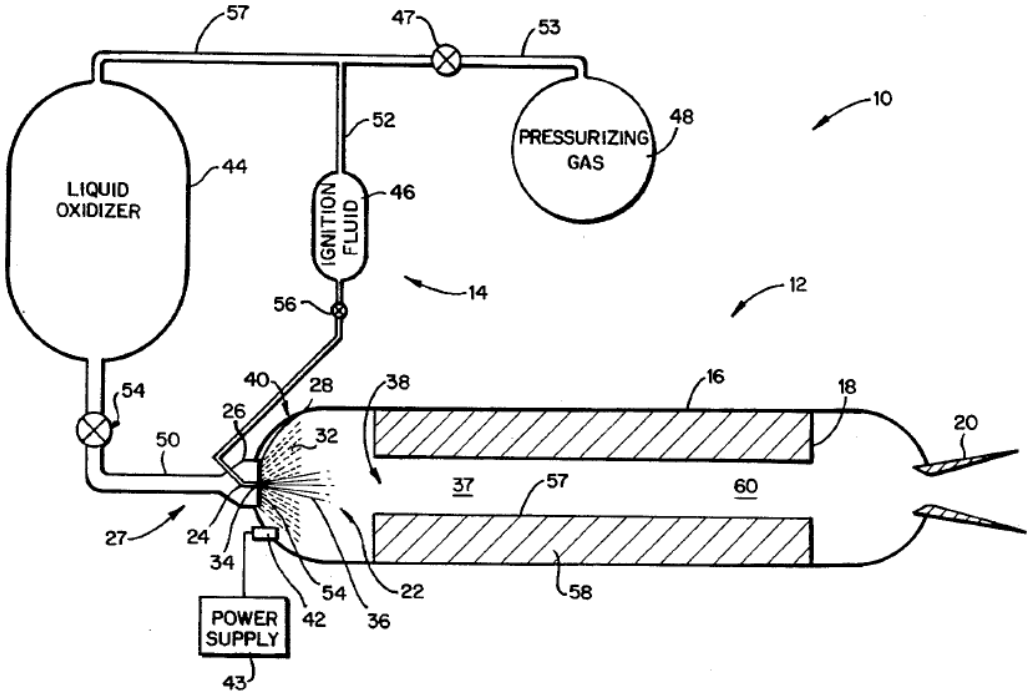

Figure 1.7: AMROC motor configuration; 26-LOX injector, 32-LOX spray, 34-ignition fluid injector, 36-ignition fluid spray (adapted from [32]).

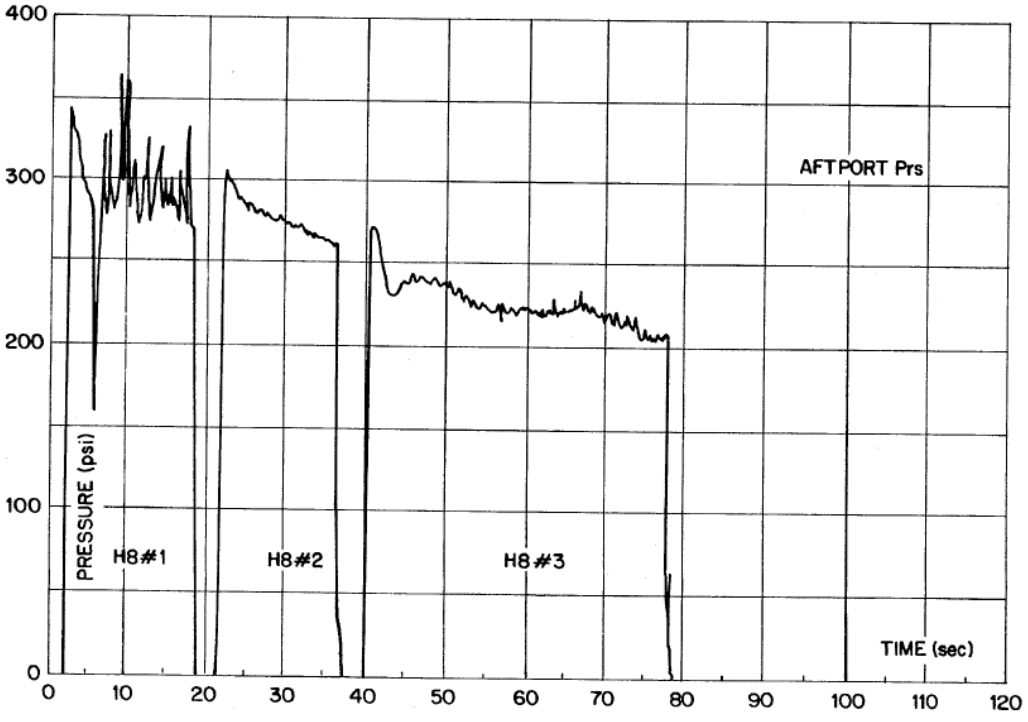

Figure 1.8: Aftport pressure profiles of three short firings (adapted from [32]).

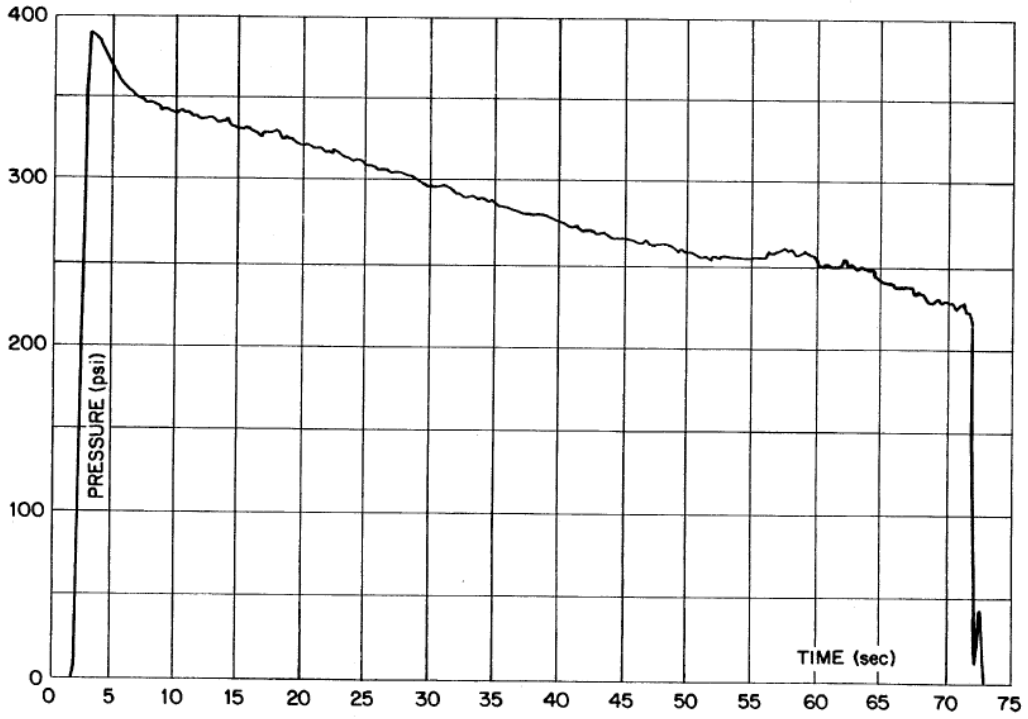

Figure 1.9: Aftport pressure of a 70-second-duration motor firing with continuous TEA injection (adapted from [32]).

1.5 Objectives and Outline of the Thesis

This thesis aims to comprehensively investigate the ignition characteristics and performance of triethylaluminum (TEA) combined with nitrous oxide (N_2O).

In Chapter 2, physical and chemical properties of TEA are given, and safety and handling procedures as well as associated risks are explained. Additionally, its reaction with nitrous oxide is investigated.

Moving to Chapter 3, design aspects of TEA injector and tank, alongside the N_2O injector is given. Then, experimental setup is detailed, and test campaign is explained. The test campaign involves two phases: 1) ignition delay and boundary determination, and 2) spray temperature measurement.

In Chapter 4, test results are presented and discussed. These results serve as the foundation for the development of an igniter motor, intended for application in hybrid rocket motors.

Chapter 2:
TRIETHYLALUMINUM

Pyrophoric materials, a subset of hypergols, ignite spontaneously and instantly upon contact with air and/or water. Common hazards associated with them include corrosiveness, teratogenicity, organic peroxide formation, and potential damage to the liver, kidneys, and central nervous system. Yet, proper handling techniques can substantially mitigate these risks and hazards. Their pyrophoricity makes these substances highly reliable ignition source, which is a crucial attribute, especially for space systems. Some examples of pyrophoric liquids are organolithiums or "Grignard Reagents" (alkyl and aryl lithium, lithium amide, sec-Butyllithium, tert-Butyllithium, lithium acetylide), organozincs (diethylzinc), aluminum alkyls (trimethylaluminum, triethylaluminum), borane alkyls (trimethylborane, triethylborane) and metal carbonyls (nickel carbonyl, iron pentacarbonyl).

Triethylaluminum (TEA) and triethylborane (TEB) are the two most common pyrophoric liquids utilized as ignition sources. TEA demonstrates lower toxicity levels than compounds containing boron or halogens [33]. Furthermore, it exhibits excellent ignition delay characteristics in comparison to TEB, yet its combustion produces aluminum oxide, which is a persistent solid that may cause pipe and orifice blockages. Conversely, the solid combustion residue from TEB is softer and less obstructive. A mixture of 15% TEA and 85% TEB by weight results in an acceptable residue while maintaining favorable ignition delay characteristics [11]. However, there exist several technical difficulties for in-space applications of pyrophoric ignition systems. For example, the cold temperature resulting from the space environment cause pyrophoric liquids to freeze in their tanks and feed systems and may increase the ignition delay, or even result in a misfire event. In addition, low temperatures of pyrophoric substances result in lower combustion temperatures which in turn reduces the amount of heat released by the combustion process. Many experiments have been conducted to investigate the conditions at which pyrophoric mixture of TEA/TEB freeze and/or cause clogging in the feed systems [34]. In this chapter, the physical and chemical properties of TEA, along with important points regarding its safety and handling, will be provided. Subsequently, its reaction with nitrous oxide will be analyzed.

2.1 Physical and Chemical Properties

TEA is a colorless organoaluminum compound with the chemical formula $Al_2(C_2H_5)_6$. It exists as a dimer at 298 K, as illustrated in Figure 2.1. TEA serves as an industrial cocatalyst in the Ziegler-Natta polymerization of olefins. Moreover, it is used as an intermediate in the production of fatty alcohols, and as an alkylating agent in the production of other organometallic compounds. General information on TEA can be summarized as follows:

- TEA ignites spontaneously on contact with air and reacts violently when exposed to water or any oxidizing agent. Additionally, it is highly reactive with various alcohols, alkalis, organic halides, acids, and bases [35] [36].
- It poses good storability at room temperature. If stored properly, i.e., under dry inert atmosphere and away from heat sources, triethylaluminum can be considered stable [37] [38].
- TEA exhibits good compatibility with aluminum, stainless steel, copper, PTFE (Teflon), FFKM, FFKM Resifluor, TPV and moderate compatibility with FKM [11] [39]. However, it is incompatible with nitrile, polychloroprene (neoprene), NBR, TPE and EPDM [40] [41]. Here, compatibility is referred to limitation in the life of the material that encounter TEA.
- It demonstrates good thermal stability such as it undergoes slow decomposition over 120°C [21]. Thermal decomposition products include hydrogen, ethylene, and elemental aluminum [38]. Combustion products are primarily carbon monoxide, carbon dioxide and metal oxide.
- Monomeric molecules of TEA are more reactive compared to dimeric molecules due to the electron deficiency of the aluminum atom [42].

Table 2.1 presents some of the physical and chemical properties of TEA. Information given have been collected from various sources [35] [38] [42] [43] [44] [45].

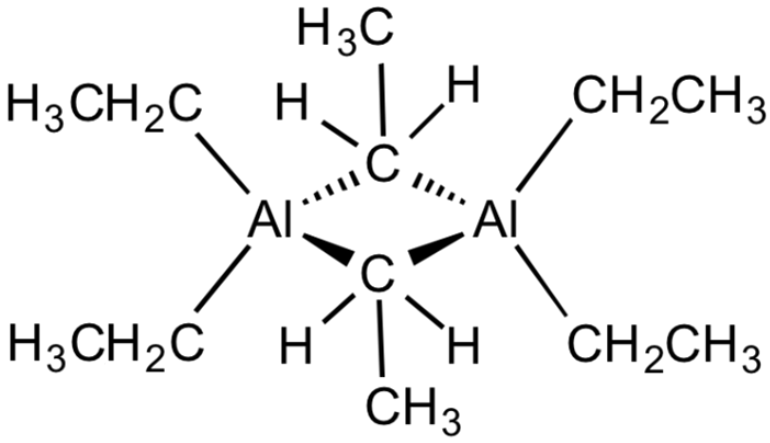

Figure 2.1: Molecular structure of TEA dimer.

Table 2.1: Physical and chemical properties of TEA.

Physical state at 25°C and 1 atm	Liquid
Melting/freezing point	-52°C
Boiling point	186°C
Vapor pressure at 25°C	0.0027 kPa
Density at 25°C	0.835 g/cm^3
Dynamic viscosity at 25°C	2.5 MPa.s
Surface tension at 28°C	0.0261 N/m
Molecular weight of the dimer	228.33 g/mol
Heat of formation of the dimer	-374.6 kJ/mol
Heat of dissociation from dimer to monomer	70.84 ± 0.96 kJ/mol
Heat of vaporization at normal boiling point	536 J/g
Constant pressure heat capacity at 25°C	239 J/mol.K
Heat of combustion	-5105.7 kJ/mol

2.2 Safety and Handling

In the realm of this thesis study, a critical focus is placed on safety and handling, particularly due to the utilization of a pyrophoric reagent, which presents significant hazards. Careful handling is necessary to ensure safe operations, which can be achieved through the implementation of various safety measures. These measures encompass the utilization of necessary Personal Protective Equipment (PPE), the implementation of appropriate engineering controls, and the selection of suitable transfer methods. Several methods, such as the cannulation method or the use of a syringe, exist for transferring a pyrophoric reagent. Transfer operations can be conducted within a fume hood or within the inert atmosphere of a glovebox, with the latter being recognized as the safer option. The glovebox is being employed in this study, facilitating a straightforward transfer process wherein the reagent is simply poured from its vessel into the designated test tank. The recommended and/or mandatory PPE includes:

- Hand protection: It's highly recommended to wear nitrile gloves beneath the glovebox gloves for safety and hygiene. Additionally, fire-resistant gloves should be worn at all times when handling the TEA vessel or working near equipment containing TEA, such as charged and/or pressurized feed lines.
- Eye protection: When working within the glovebox, wearing splash goggles or safety glasses is highly recommended. However, a face shield becomes mandatory when conducting operations outside the glovebox, especially while handling the TEA vessel or during pre- and post-test procedures like opening valves or securing the test cell. It's important not to wear contact lenses while working with this substance.
- Clothing: Synthetic fabrics should be avoided. Additionally, open-toe shoes are not allowed. While it's recommended to use fire-resistant shoe materials, it's not mandatory. During glovebox operations, wearing fire-resistant coveralls is highly recommended. However, when working with TEA outside the glovebox, wearing fire-resistant coveralls becomes mandatory.

2.2.1 General Safety Measures and Equipment Preparations

- Emergency eyewash and safety showers should be within 10 seconds of distance.
- Proper PPE must be worn all the time.

- The recommended fire extinguisher is the standard dry powder (ABC) type, which is the most effective means of controlling clothing fires. It's essential that the extinguisher remains within arm's reach.
- At least two people should be present when working with TEA, following the Buddy System. Additionally, at least one person with knowledge and experience in handling pyrophoric reagents must be present.
- Standard Operating Procedure (SOP) must be prepared in accordance with the transfer and test operations and must be strictly followed at all times.
- Materials that come in contact with the reagent must be compatible with it.
- All materials, including disposable gloves, wipers, and bench paper contaminated with pyrophoric chemicals, should be sealed in an appropriate container or plastic bag before being removed from the glovebox and disposed of as hazardous waste.
- Any container with a residue of reactive materials should never be left open to the atmosphere. The contaminated waste should not be left in the open laboratory but must be properly and immediately contained to prevent fires.
- Any excess chemical should never be returned to the original container. Even small amounts of impurities introduced into the container can potentially cause a fire or explosion. It's essential to quench any excess chemical properly and label it as “hazardous waste”.
- All flammable materials and objects must be removed from the working area. TEA must be kept away from any kind of heat source.
- The reagent vessel must always be secured with clamps. Tanks should be sealed when not in use and stored within the inert atmosphere of the glovebox. TEA reagent vessels should not be removed from the glovebox unless absolutely necessary.
- Instruments and equipment used inside the glovebox must be vacuum-compatible to prevent potential spills of the chemical inside the antechamber.
- All glassware and equipment, including tanks and fittings, must undergo oxygen cleaning to prevent contamination. Subsequently, they should be dried in an oven at 60°C for a minimum of four hours and then cooled either in an inert atmosphere or in a desiccator.

2.2.2 Transfer and Quenching/Cleaning Procedures

As previously stated, the transfer of TEA from its vessel to the test tank occurs within the inert atmosphere of the glovebox, as depicted in Figure 2.2. The reagent is transferred by slowly and gently pouring it through a funnel into the designated test tank. Simultaneously, the precision balance is checked to monitor the amount of TEA being transferred. A visual demonstration of this transfer procedure is presented in Figure 2.3. Important points regarding the transfer procedure are as follows:

- O_2 levels must be maintained below 2.0 ppm to prevent TEA from smoking.
- H_2O levels must be kept lower than 0.1 ppm due to TEA's sensitivity to moisture.
- Any glassware and instrumentation that come in contact with TEA must be properly cleaned and dried before the transfer procedure.
- Following the transfer, the TEA-contaminated glass funnel should be immersed in sequential chemical baths including toluene, isopropanol, and methanol, respectively to quench any residue (Figure 2.4).

The quenching process for the residue in the TEA vessel involves the following steps:

- 40-50 ml of toluene, isopropanol and methanol must be prepared separately in individual glass bottles.
- Initially, toluene must be poured into the residue TEA through a funnel. It is important that toluene contacts each surface of the TEA vessel to quench any residue. Then, TEA/toluene solution must be transferred into an empty glass bottle.
- Isopropanol and methanol must be slowly added to the solution, respectively, while stirring gently.
- The bottle containing the final solution must be properly sealed and labeled as hazardous waste before bringing out of the glovebox.

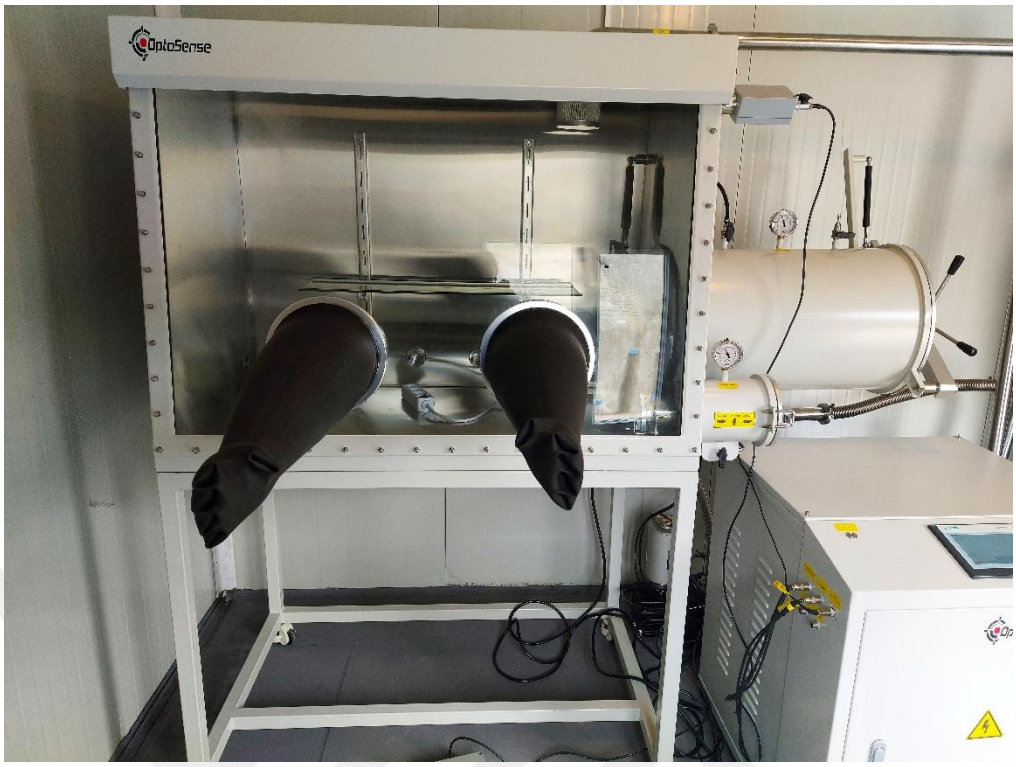

Figure 2.2: Glovebox system.

Figure 2.3: Transfer procedure.

Figure 2.4: Chemical baths used for quenching.

2.2.3 Potential Hazards

Pyrophorics are prone to accidents and can cause serious injuries. Potential hazards, including spills during transfer and handling, as well as possible leaks during testing, pose significant risks. A comprehensive risk assessment for both glovebox and test operations is summarized in Table 2.2.

Table 2.2: Risk assessment.

Situation/Action/Task	Potential hazard	Risk minimization
Removing pyrophoric chemicals from the glove box	The container with the chemical may leak or accidentally open or rupture, causing immediate fire hazards, risk of serious injury or burn damage.	Wear face shield, fire resistant gloves and coverall. Carefully open the hatch a few millimeters and look for smoke. If smoke is detected, immediately close the hatch, and bring the container back into the glove box. Purge the antechamber before. If no smoke, carefully and slowly open the hatch fully.

Spilling flammable/ pyrophoric chemicals inside the glove box	May cause fire and explosion hazards during cleaning or subsequent use of the antechambers.	If the spill is small, carefully quench the spill by dropping toluene, isopropanol, and methanol, respectively. If the spill is large, remove any flammable material away the spill immediately. Carefully quench the spill with copious amount of toluene, isopropanol, and methanol, respectively. In both cases, collect the quenched residue with paper towel. Double bag the contaminated materials and label as hazardous waste.
Rupturing/ puncturing the gloves	If the hole is larger than about 1 mm, it may increase the oxygen and moisture levels.	Seal the glove with a tape until the reagent inside the glovebox is secured. Change the gloves immediately. Always keep a pair of gloves ready for such cases. Use of additional gloves on top of the glovebox gloves may mitigate the risk of puncturing when handling sharp objects.
Using chemicals incompatible with the glovebox gloves	Certain chemicals may dissolve, react, or soften the gloves which can lead to direct skin contact to the hand through the glove.	Make sure that the chemicals used are compatible with the glove material. Use of additional gloves on top of the glovebox gloves may mitigate the risk.
Manuel valve opening during transportation and/or integration	May cause the reagent to leak. Smoke and/or fire can be detected.	If smoke detected, close the valve carefully while wearing the necessary PPE during the time. If fire detected, secure the area, and use the proper fire extinguisher until the reaction is under control. Always plug the valves or fittings during transportation. Always use additional isolation valves to prevent any hazard.

Loosen fitting	May cause the reagent to leak. Smoke can be detected. If the tanks and lines are pressurized above the atmospheric level, this may lead to an external fire at the leakage locations.	If smoke detected, tighten the loosen fitting carefully while wearing the necessary PPE during the time. If leakage occurs during test, wait until the sequence is over. Evacuate the remaining TEA and purge the tank/lines until the fire and/or smoke vanishes. Double check each fitting connection before pressurizing the system.

2.3 Reaction with Nitrous Oxide

As previously mentioned, TEA is highly reactive with oxidizers, and the heat generated from this combustion reaction can be utilized as an ignition source for a propulsion system. In the scope of his study, combustion characteristics of TEA with N_2O will be investigated.

N_2O is a colorless and odorless fluid with low toxicity, making it relatively safe to handle. It exhibits a high vapor pressure at room temperature, a feature that allows the feed system to self-pressurize. As a result, it is widely preferred in propulsion systems due to this self-pressurizing characteristic, eliminating the need for complex pressurizing systems like turbopumps or pressurized tanks filled with gases such as helium or nitrogen. These additional systems would otherwise contribute to the overall weight of the system. The properties of N_2O are detailed in Table 2.3 [46].

Table 2.3: Properties of N_2O.

Vapor pressure at 25°C	5.6518 MPa
Normal boiling point	184.7 K
Molecular weight	44.013 g/mol
Heat of formation, gas	82.05 kJ/mol
Heat of formation, liquid	65.1 kJ/mol

2.3.1 Stoichiometric O/F Ratio

In a combustion reaction, the stoichiometric ratio refers to the balanced ratio of the fuel and oxidizer required for complete combustion to occur. This ratio ensures that all the fuel is consumed by the available oxygen without any excess of either fuel or oxygen remaining after the reaction. Products of a stoichiometric combustion are usually carbon dioxide and water. However, in the case of TEA/N_2O, additional products such as nitrogen and aluminum oxide must be included when establishing the stoichiometric reaction equation. Taking these considerations into account, stoichiometric reaction for the combustion of TEA with N_2O can be established as Eq. 2.1.

$$C_{12}H_{30}Al_2 + 42N_2O \rightarrow 12CO_2 + 15H_2O + 42N_2 + Al_2O_3 \quad (2.1)$$

From above equation, stoichiometric O/F ratio can be calculated as 8.1.

2.3.2 Performance Parameters

There are several performance parameters associated with propellant combinations, including characteristic velocity (c*), combustion temperature (T_c), and, as previously emphasized, specific impulse. Figure 2.5 demonstrates the performance parameters of the TEA/N_2O reaction at various chamber pressures (P_c). All calculations were performed using NASA CEA program. The black circle markers in the first graph where P_c is 1 bar indicate the O/F ratios that the ignition delay tests were conducted. These tests will be outlined later in Chapter 3.

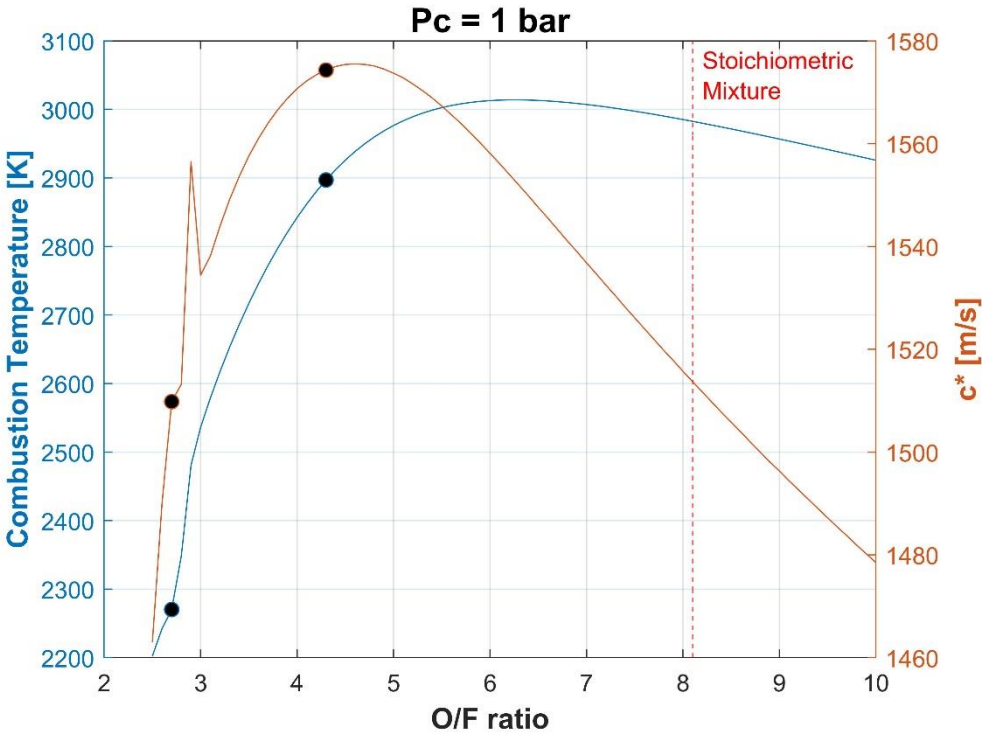
Pc = 1 bar
Stoichiometric Mixture
Combustion Temperature [K]
c* [m/s]
O/F ratio
3100
3000
2900
2800
2700
2600
2500
2400
2300
2200
1580
1560
1540
1520
1500
1480
1460
2
3
4
5
6
7
8
9
10

(a)

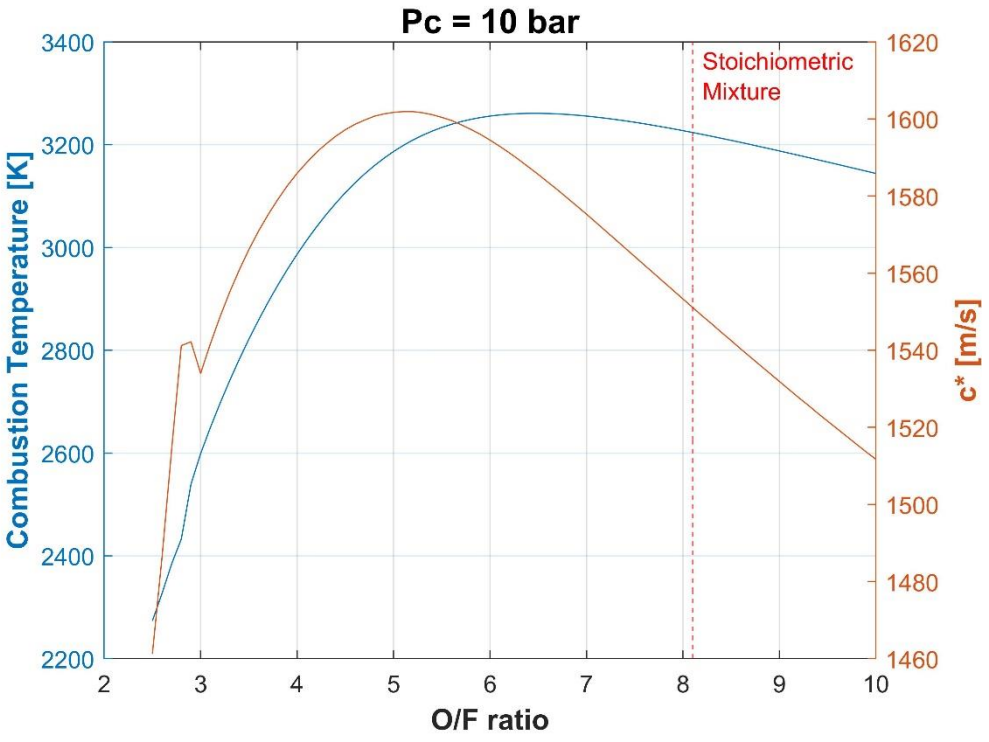
Pc = 10 bar
Stoichiometric Mixture
Combustion Temperature [K]
c* [m/s]
O/F ratio
3400
3200
3000
2800
2600
2400
2200
1620
1600
1580
1560
1540
1520
1500
1480
1460
2
3
4
5
6
7
8
9
10

(b)

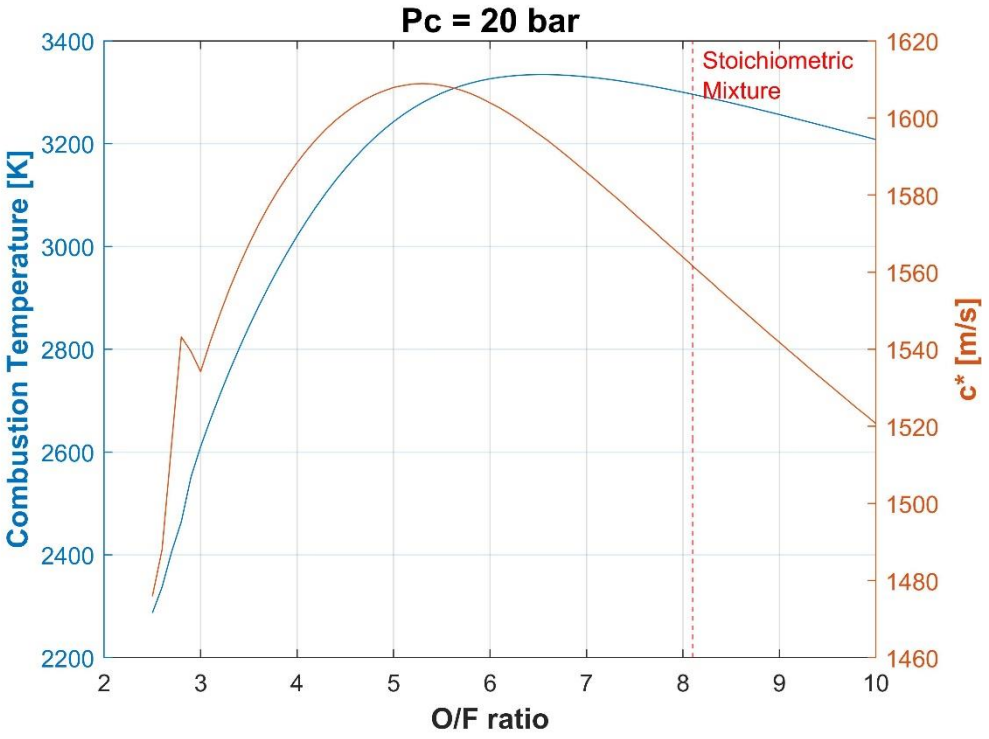

(c)

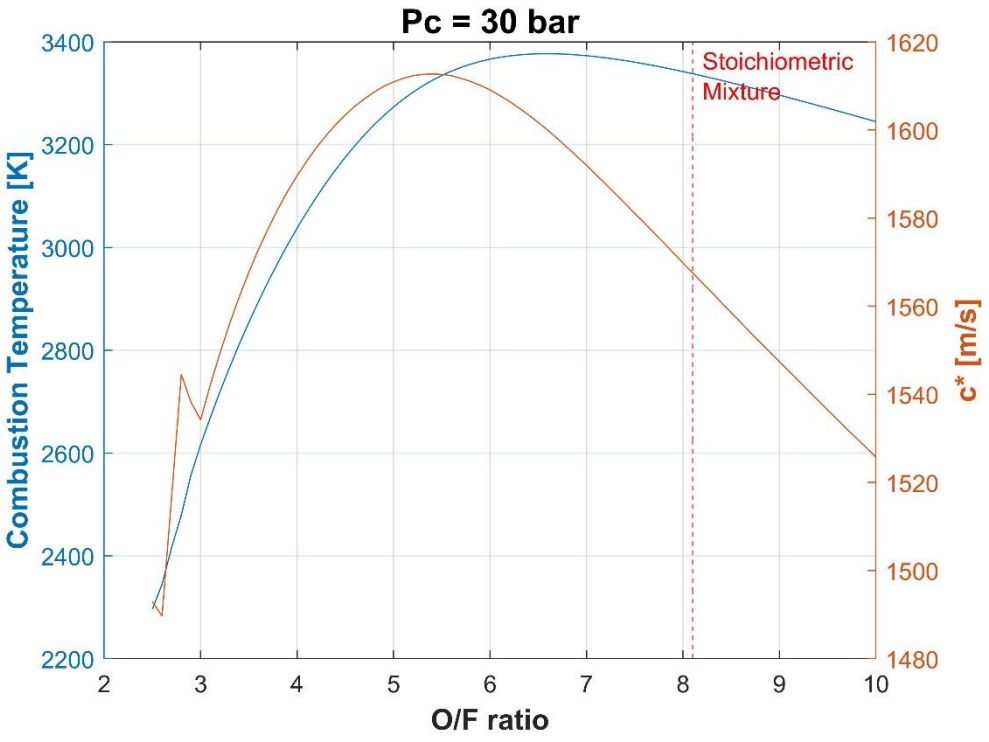

(d)

Figure 2.5: Variation of T_c and c* for pressure values (a) P_c = 1 bar, (b) Pc = 10 bar, (c) Pc = 20 bar, (d) Pc = 30 bar.

It can be seen from the graphs that O/F ratios corresponding to the maximum values of both T_c and c* are lower than the stoichiometric O/F ratio, as expected. Additionally, O/F ratio corresponding to the maximum T_c is higher than the one that of maximum c*, which is also expected. In c* plots, “spikes” have been observed. “Spikes” or “data gaps” in NASA CEA calculations are common when dealing with fuels that contain metal additives or molecules that include metals, due to the complexity of reactions involving metals. Metals in fuels or molecules can significantly influence the thermochemical properties and reaction pathways during combustion processes. At Table 2.4, maximum T_c and c* values along with the corresponding O/F ratios for different chamber pressures are summarized.

Table 2.4: Maximum T_c and c* with corresponding O/F ratios for different chamber pressures.

Pressure	Maximum T_c	Corresponding O/F	Maximum c*	Corresponding O/F
1 bar	3013.80 K	6.3	1575.5 m/s	4.6
10 bar	3260.85 K	6.5	1601.9 m/s	5.1
20 bar	3334.37 K	6.5	1608.9 m/s	5.3
30 bar	3376.85 K	6.6	1612.7 m/s	5.4

It can be observed from the Figure 2.5 and Table 2.4 that, with increasing pressure, the maximum points tend to shift towards higher O/F ratios. Furthermore, the maximum values of both T_c and c* also increase as pressure rises.

Another crucial parameter for an igniter is the energy output rate,

2.3.3 Comparison with Various Igniters

A frequently used ignition system in hybrid rockets involves employing a small-scale hybrid motor to ignite a larger one, as previously mentioned. Typically, this system employs the same oxidizer for both the main and igniter motors, aiming to reduce system complexity and overall mass. Figure 2.6 illustrates the performance parameters of reactions involving paraffin/N_2O, HDPE/N_2O, PA6-6/N_2O and Al+Paraffin/N_2O at a P_c value of 20 bar. Additionally, Figure 2.5 summarizes the maximum T_c and c* values

along with their corresponding O/F ratios. All parameters are calculated using the NASA CEA program in a similar manner as TEA/N_2O calculations.

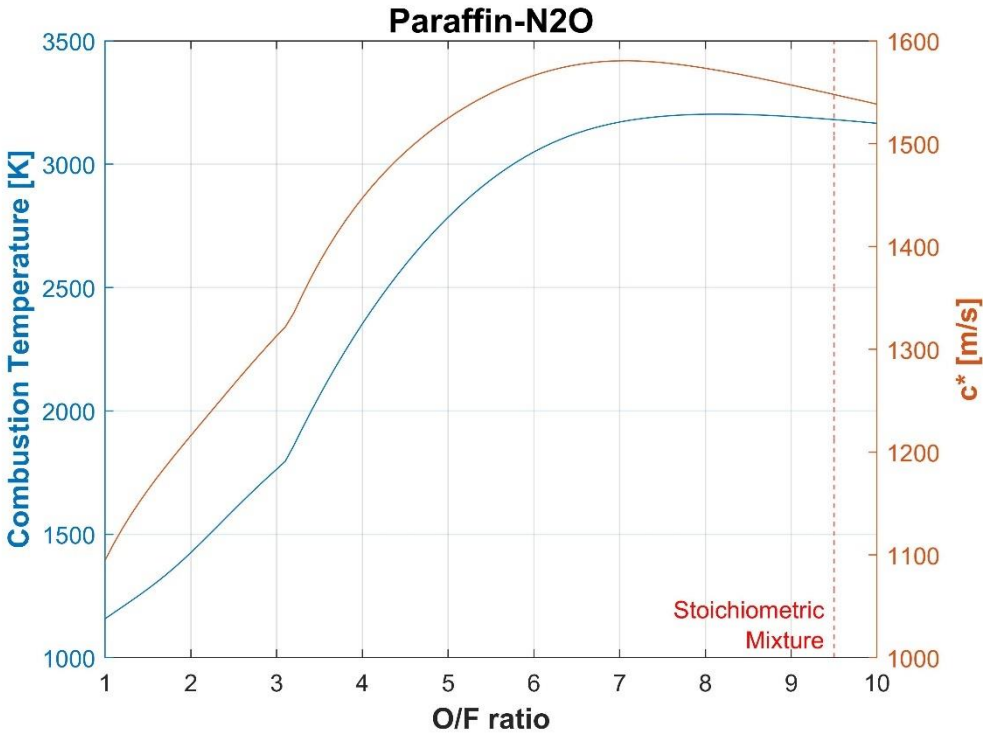

(a)

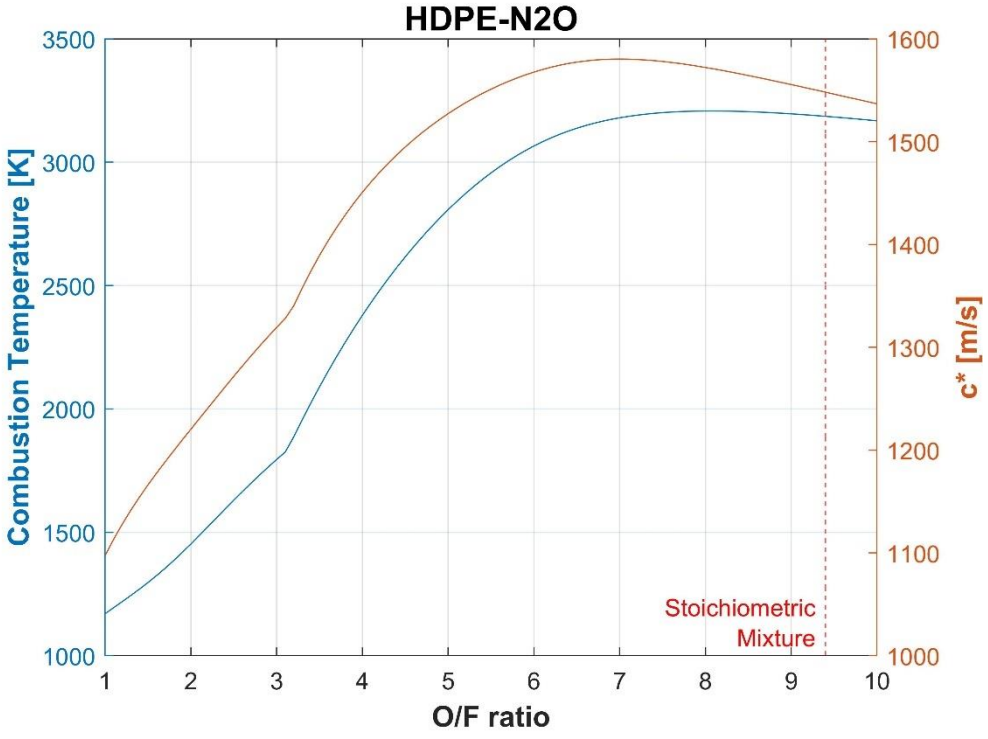

(b)

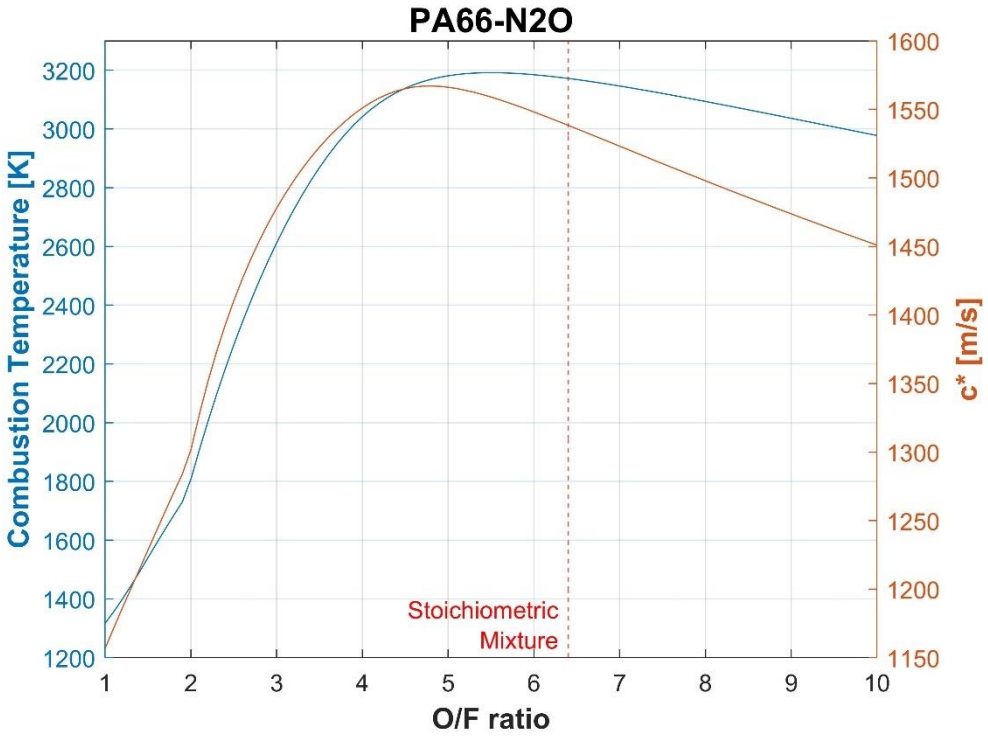

(c)

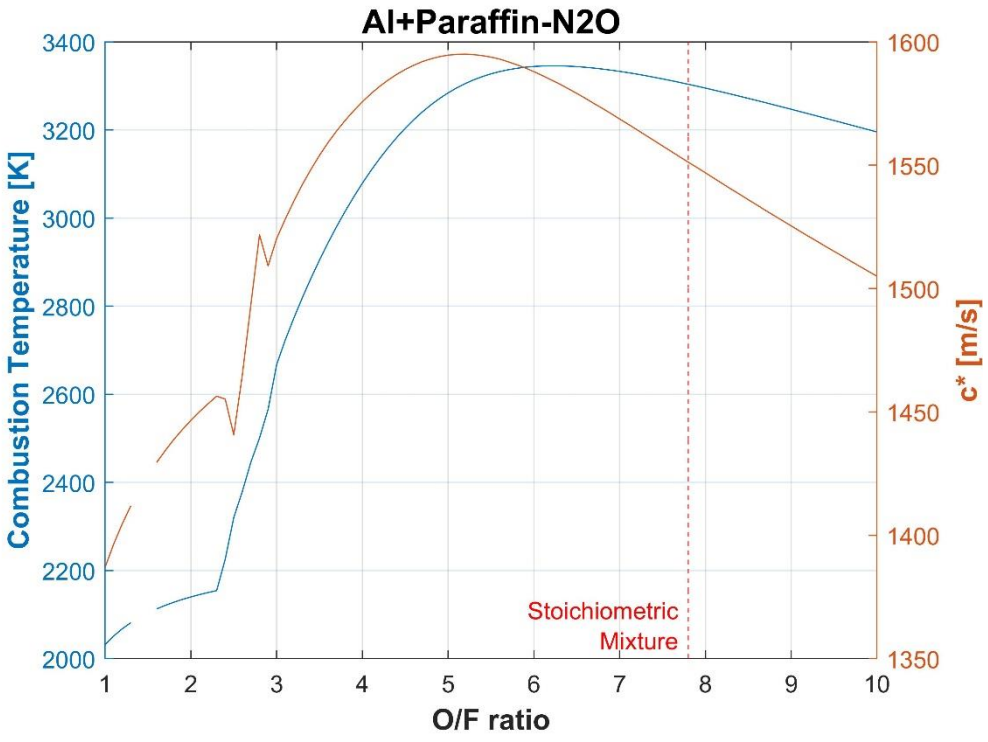

(d)

Figure 2.6: Variation of T_c and c* at P_c = 20 bar for (a) Paraffin/N_2O, (b) HDPE/N_2O, (c) PA6-6/N_2O, and (d) Al+Paraffin/N_2O.

Table 2.5: Maximum T_c and c* with corresponding O/F ratios for different propellant pairs.

Propellant Pair	Maximum T_c	Corresponding O/F	Maximum c*	Corresponding O/F
Paraffin/N_2O	3202.69 K	8.2	1580.6 m/s	7.1
HDPE/N_2O	3207 K	8.1	1580.13 m/s	7
PA6-6/N_2O	3191.47 K	5.5	1567 m/s	4.8
Al+Paraffin/N_2O	3345.47 K	6.2	1595 m/s	5.2

Here, the fuel mixture “Al+Paraffin” is essentially paraffin fuel with aluminum (Al) powder additive. Comparing the data from Table 2.4 and Table 2.5, it's evident that TEA/N_2O demonstrates relatively better performance than paraffin/N_2O, HDPE/N_2O, and PA6-6/N_2O pairs. However, performance parameters of TEA/N_2O are similar to that of Al+Paraffin/N_2O, with a slightly lower Tc and slightly higher c*. For a better comparison, the mass fraction of Al in “Al+Paraffin” fuel mixture is equal to the mass fraction of Al in a TEA dimer molecule. Also, similar “spikes” to that of TEA/N_2O and additional “data gaps” have been observed at low O/F ratios. This is quite common for fuels with metal additives and/or molecules that include metals. These spikes or gaps often occur due to the complexity of reactions involving metals, as previously explained.

Chapter 3:
EXPERIMENTAL EVALUATION

Ignition delay is a critical parameter in igniter design, as previously highlighted. Furthermore, injector configuration parameters, particularly impingement (or momentum) angle, may significantly influence design considerations. This study focuses on analyzing the ignition delay characteristics of the TEA/N_2O propellant combination across various O/F ratios and impingement angles. The insights gained from this analysis will be important in shaping the conceptual design of an igniter system.

This chapter presents detailed information regarding the design of essential system components, including injectors and tank. Additionally, it offers a comprehensive overview of the test bench, instrumentation, and hardware utilized throughout the test campaign. Lastly, it provides a thorough explanation and outline of the test program.

3.1 Design

3.1.1 TEA Injector

The isometric and section views of the TEA injector are depicted in Figure 3.1. The injector was intentionally designed resembling a fitting with NPT threads, enabling easy integration into feedlines or assembly to various system components, such as the motor case or pre-combustion chamber. Manufactured from AISI 316L stainless steel, the injector demonstrates good compatibility with TEA, as previously indicated.

Orifice diameter was chosen as 0.6 mm since orifices with diameters larger than 0.7 mm results in reactive stream separation for hypergolic propellants [47]. In addition, small orifices may be clogged due to the accumulation of aluminum oxide and cannot be used in the case of multiple ignitions. Hence, the selected orifice diameter aligns well with these constraints. Discharge coefficient (C_d) is determined as 0.9 which will be discussed later in this chapter.

3.1.2 N_2O Injector

The CAD model of the N_2O injector is shown in Figure 3.2. Similar to the TEA injector, this component was also manufactured using AISI 316L stainless steel. However, it was designed differently, featuring 3/8 Swagelok tubing for integration into

the feed system and 3/8 NPT threads for assembly with the motor case or pre-combustion unit.

The orifice diameter for this injector was chosen as 0.8 mm, with two variations utilizing 3 and 4 orifices respectively. The reason behind this choice will be explained in detail in a later section of this chapter.

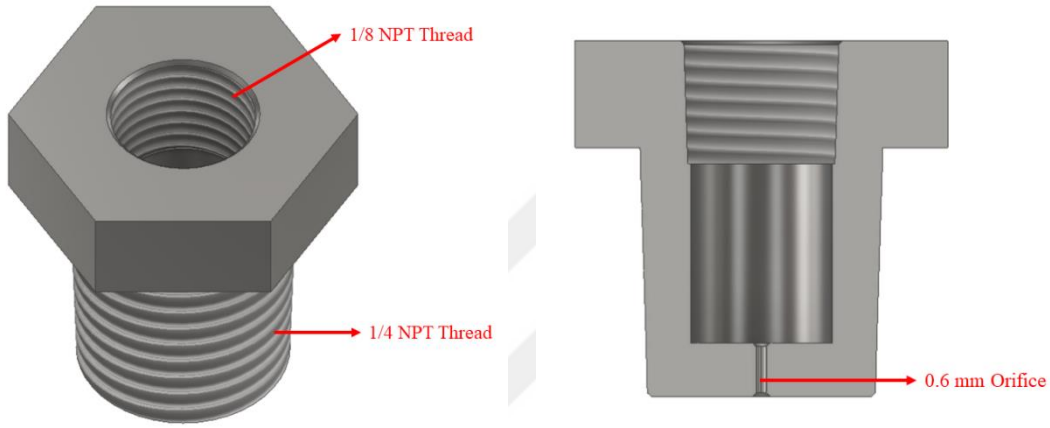

Figure 3.1: TEA injector.

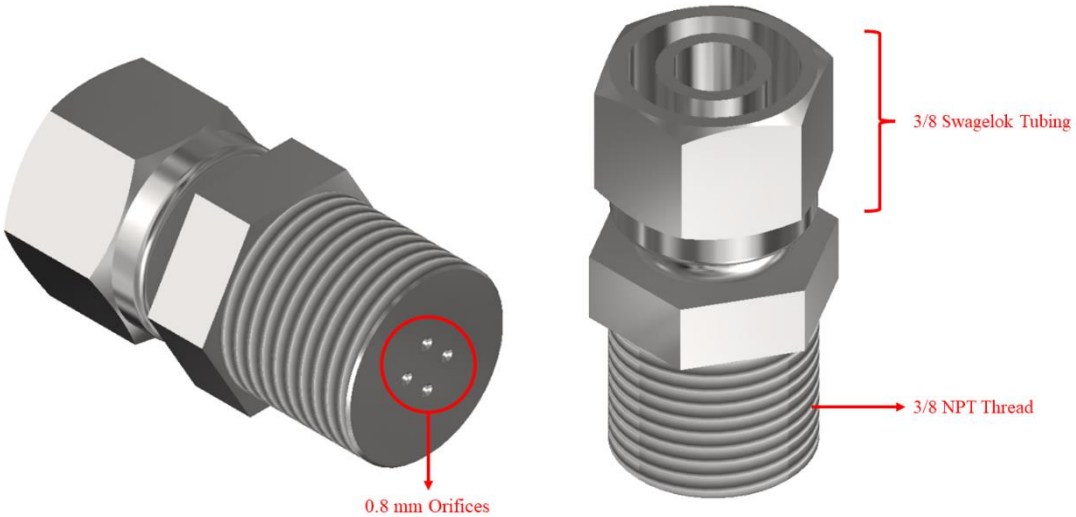

Figure 3.2: N_2O injector

3.1.3 TEA Tank

The design of the tank is depicted in Figure 3.3. It comprises two dome parts with 1/8 NPT threaded connections and a body part, all manufactured from AISI 316L stainless steel. With its measured thickness, the estimated burst pressure is approximately 750 bars. The Maximum Expected Operating Pressure (MEOP) is set at 60 bars, resulting in a Safety Factor (SF) of 12.5.

Due to the presence of two welded joints on the tank, there is a possibility that both the burst pressure and the consequently SF may slightly decrease from their intended values. However, the SF remains notably high despite this potential reduction. The tank underwent hydrostatic testing up to a pressure of 100 bars, which proved successful as no deformation or damage was observed.

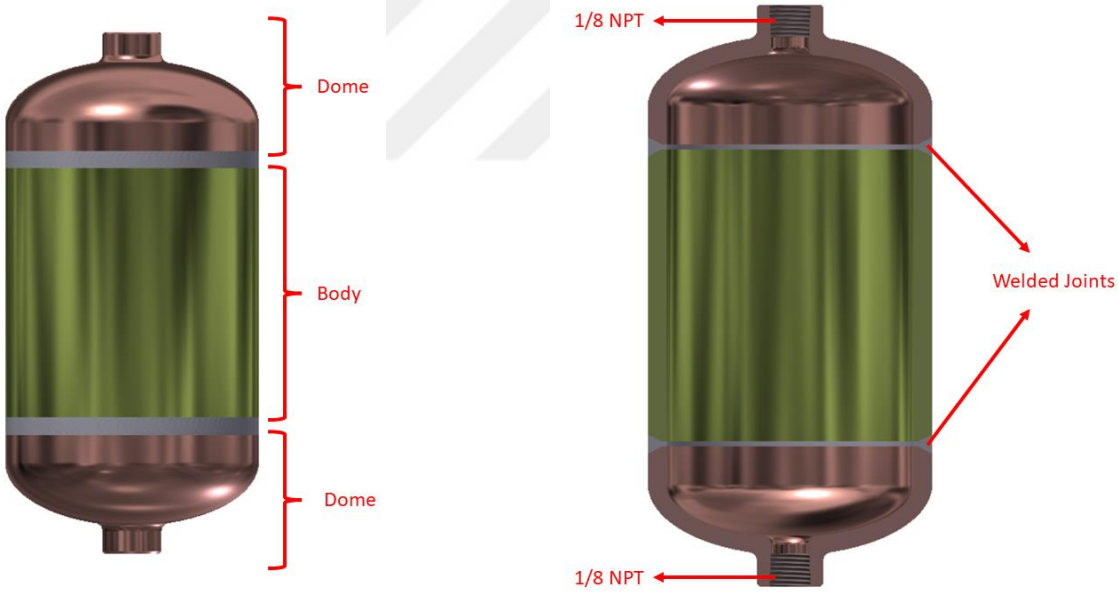

Figure 3.3: TEA tank.

3.2 Experimental Setup

The tests were conducted in a multi-purpose motor static fire test bench located in the test facility of DeltaV Space Technologies, Inc. Figure 3.4 depicts the Piping and Instrumentation Diagram (P&ID) of the test setup. The setup comprises two industrial nitrogen (N_2) tubes for pressurization and purging, alongside one N_2O run tank and one TEA run tank. The setup incorporates three distinct lines: an N_2O line, a pressurization and sequential TEA line interconnected, and a purging line that joins the TEA line upstream of the TEA injector. Following each N_2 tube, a pressure regulator is connected to maintain the operational pressure levels within the feedlines. The system consists of eight manual valves (MV) used for isolation and venting purposes, complemented by four automatic valves (AV) facilitating pressurization, isolation, and primary flow control.

To measure the temperature within the mixed spray, K-type thermocouples (TC) with exposed probes and maximum measurement value of 920°C were employed. Additionally, four pressure transducers (PT) with a range of 0-70 bars and $< \pm 0.5\%$ measuring accuracy and $< \pm 0.05\%$ repeatability were integrated into the tanks and upstream of the injectors for pressure measurement. Test data were recorded using the National Instruments Data Acquisition System (DAQ) in conjunction with LabVIEW software. The DAQ system operates at a sampling rate of 5120 Hz. Chronos 1.4 High Speed Camera operating at a frame rate of 1057 fps was utilized to calculate the ignition delay. Figure 3.5 illustrates the experimental setup.

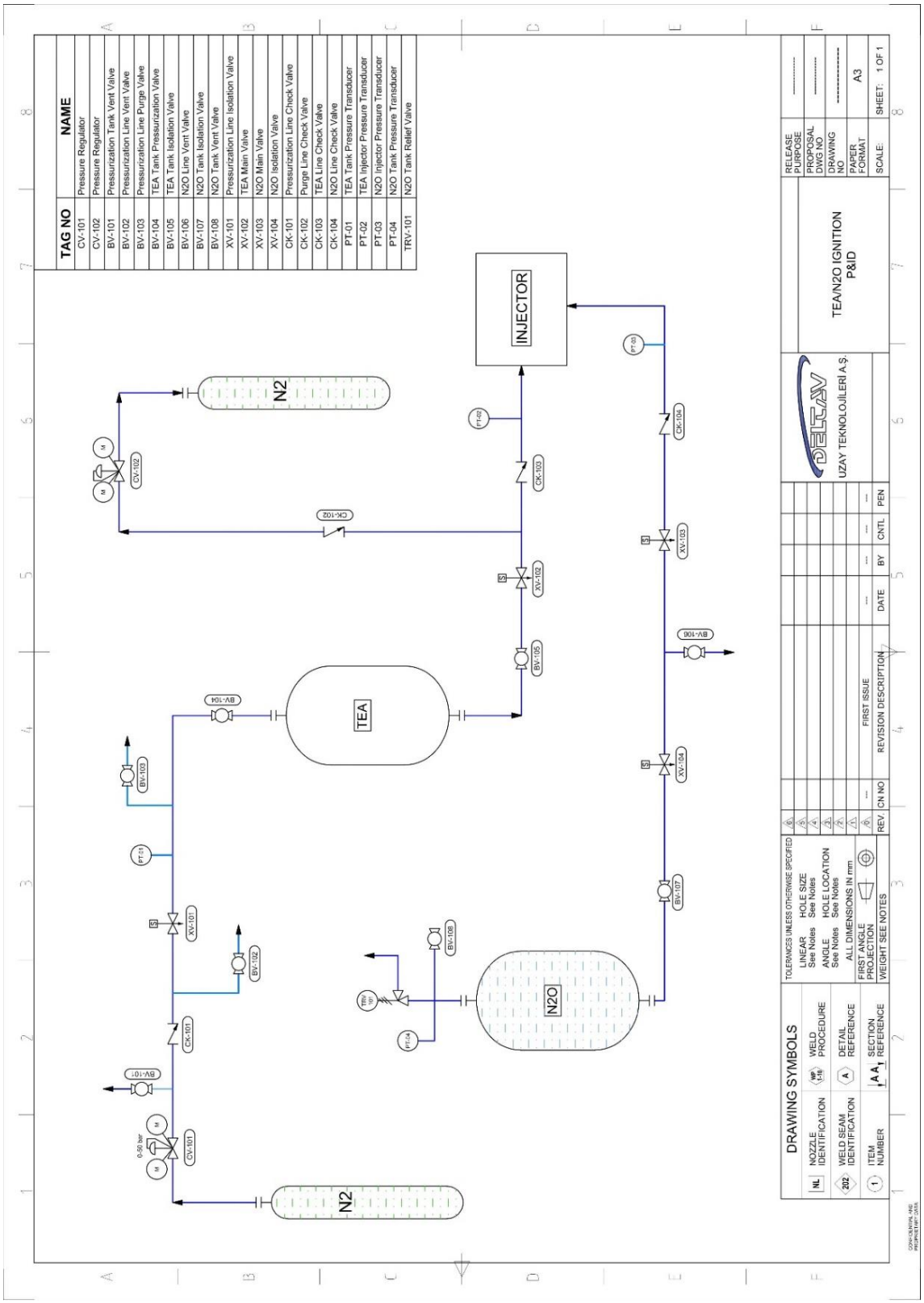

Figure 3.4: Test setup P&ID.

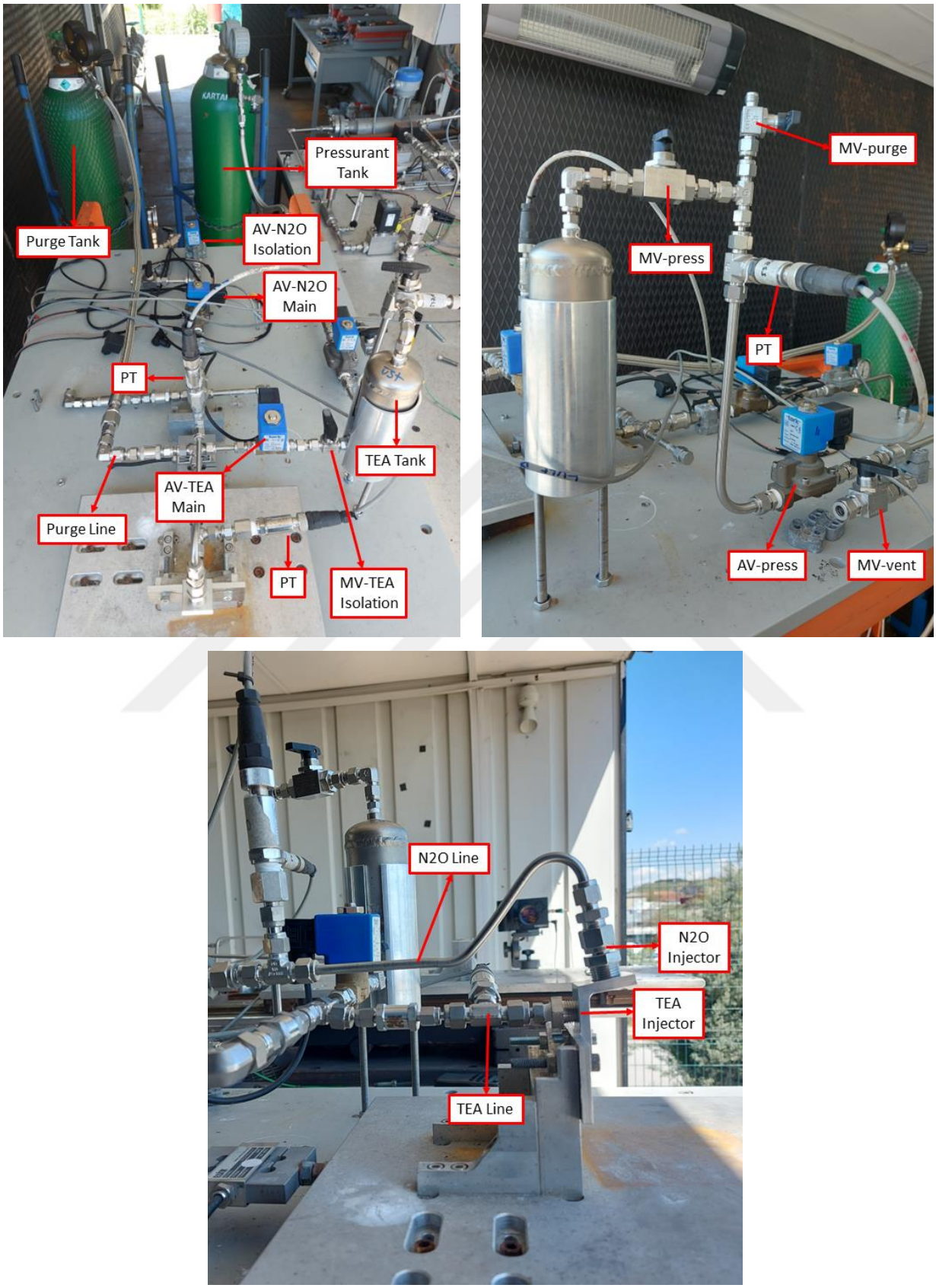

Figure 3.5: Experimental setup.

3.3 Test Campaign

The test campaign is designed to investigate the ignition delay characteristics of impinging TEA-N_2O jets. The primary objective is to determine the ignition boundary for a specific O/F ratio by varying the impingement angle. Furthermore, an additional experiment has been conducted to have an insight about the reaction downstream of the impingement points, utilizing temperature measurements from the mixed spray. The general test parameters are detailed in Table 3.1.

Table 3.1: Test parameters.

Tank Pressure N_2O	47-50 bar
Tank Pressure TEA	18-22 bar
Mass Flow Rate N_2O	37-62 g/s
Mass Flow Rate TEA	13-15 g/s
O/F Ratio	2.64-4.35
Burn Time	2-6 seconds

3.3.1 Ignition Delay and Boundary Determination

Test matrix for the ignition delay and boundary determination tests are outlined in Table 3.2. Here, for each specific O/F ratio, ignition delay values were calculated for various impingement angles, starting from 90° and going down gradually until the angle where no ignition occurred, and ignition boundary was determined. To provide the given O/F ratios, two N_2O injectors with different orifice numbers were employed: three-orifice-injector for an average O/F ratio of 2.7 and four-orifice-injector for an average ratio of 4.3, as previously specified, whereas the TEA injector diameter and number were kept the same through the entire campaign. To ensure accurate jet impingement angles, injector brackets with specific angles were manufactured and underwent quality control. As an example, 3D model of 60° bracket is shown in Figure 3.6, and the corresponding ignition test is given in Figure 3.7.

To purge air from the TEA lines before and after the test runs, the N_2 purge supply remains open for the entire operation duration. This process flushes air from the lines before the test and clears any remaining TEA from the lines and injector after the test.

Additionally, the TEA tank operates in regulation mode, maintaining a constant pressure during the test run. The test sequence involves the N_2O main valve opening at T+0 for 5.8 seconds, followed by the TEA valve opening at T+4 for a duration of 2 seconds. Notably, the N_2O flow precedes the TEA flow by 4 seconds, and they flow together for 1.8 seconds. When the N_2O valve first opened, a sudden pressure drop occurs inside the tank, leading to a "build-up" phase in mass flow rate. To make sure that the N_2O reaches its steady mass flow rate value, and the tank pressure stabilizes, a 4-second delay was implemented between the opening of the two main valves.

Table 3.2: Test matrix.

O/F Ratio	Impingement Angle
2.7	30°
	40°
	50°
	60°
	70°
	80°
	90°
4.3	72°
	74°
	76°
	78°
	80°
	90°

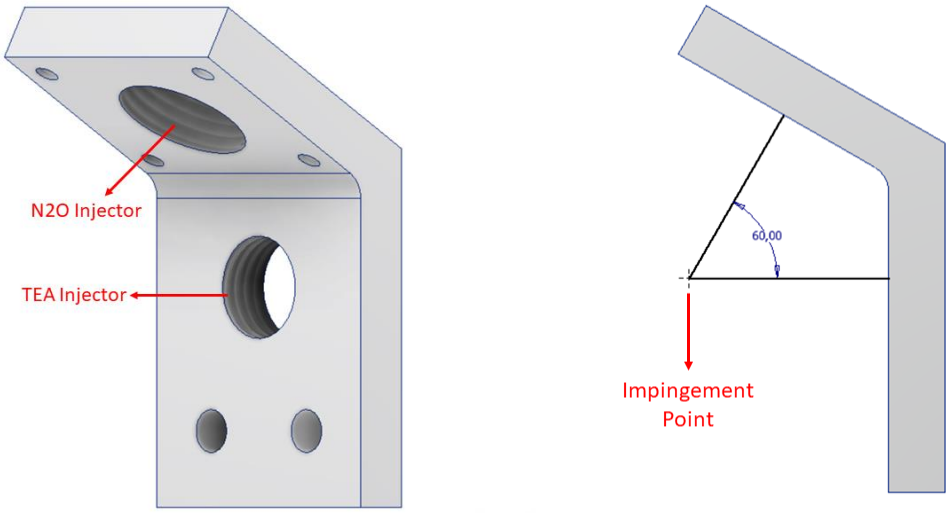

(a) (b)

Figure 3.6: 3D model of 60° bracket (a) isometric view, (b) side view.

Figure 3.7: 60° ignition test with O/F ratio of 2.76.

3.3.2 Mixed Spray Temperature Measurement

During the ignition delay and boundary determination tests, it was observed that the flame base occurs at some distance downstream the impingement point, as depicted in Figure 3.7. This is an expected phenomena for impinging hypergolic streams in a mixing condition [48], a topic that will be further discussed later.

To gain insight into the mixed spray between the impingement point and the flame base, three equally spaced thermocouples (TC) with exposed probes were positioned within that region, as illustrated in Figure 3.8. The test was conducted at an O/F ratio of 2.76 with a 60° momentum angle, a preferred value for impinging injectors [47]. Moreover, previous observations during ignition delay tests indicated that this O/F ratio - impingement angle pair demonstrates favorable mixing characteristics.

Similar to the ignition delay and boundary determination tests, the TEA tank operated in regulation mode, maintaining constant pressure throughout the test run. The test sequence commenced with the N_2O main valve opening at T-0 for 7.8 seconds, followed by the TEA valve opening at T+2 for a duration of 6 seconds. Notably, the N_2O flow preceded the TEA flow by 2 seconds, and they flowed together for 5.8 seconds. The corresponding ignition test details are provided in Figure 3.9.

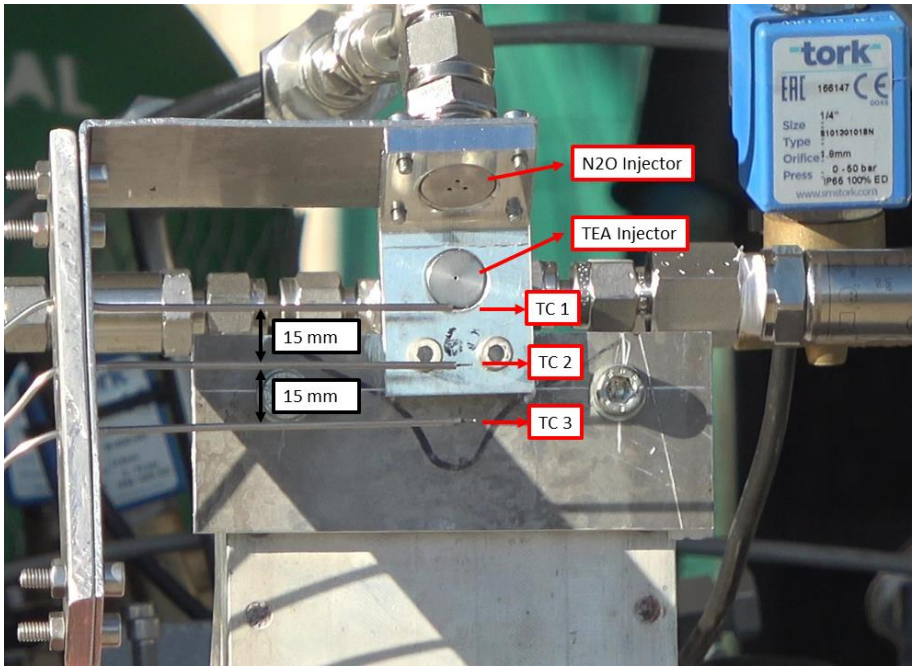

Figure 3.8: Spray temperature measurement setup.

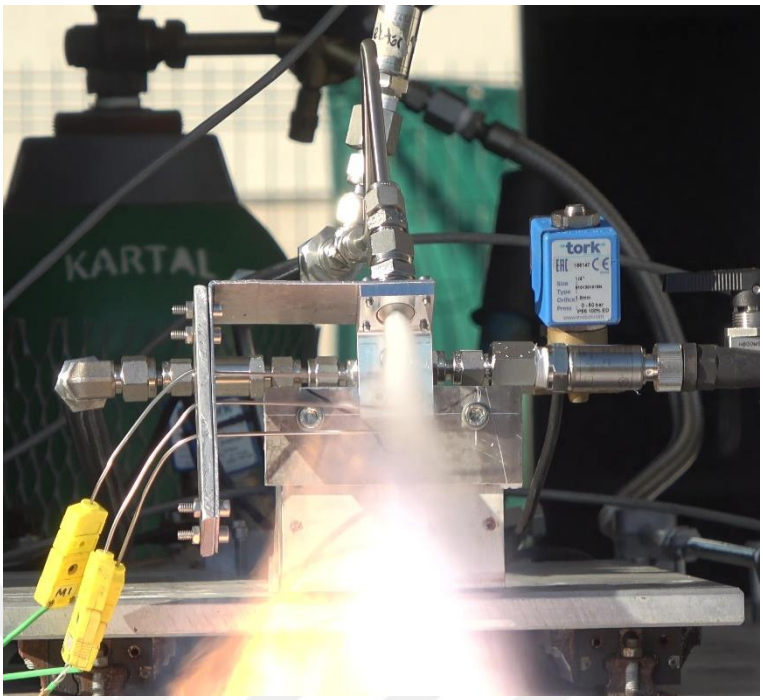

Figure 3.9: The ignition test for spray temperature measurement.

3.3.3 Data Analysis

All test data underwent processing and analysis through MATLAB software. Collected pressure and temperature data were examined to obtain the mean test values, as well as to investigate the transient behavior.

Ignition delay times were calculated utilizing a high-speed camera recording at 1057 frames per second (fps). This involved determining the number of frames between the moments when the TEA jet impinged the N_2O stream and the first observed flame. The ignition delay time was then computed by dividing this difference by the frame rate.

For calculating the N_2O mass flow rate, the tank's mass was measured both before and after each test, and the total consumed mass was divided by the flow time. When upstream pressure and temperature remain relatively constant during the test run, the instantaneous flow rate closely aligns with its average value since the flow rate of N_2O depends on these upstream conditions. The TEA flow rate for each test was computed using Eq. 3.1.

$$\dot{m} = C_d A \sqrt{2\rho\Delta P} \tag{3.1}$$

Here, A_c is the injector orifice area, ρ is the density of TEA and ΔP is the pressure drop across the injector which obtained from test data. This equation is known to predict the mass flow rate of incompressible liquids with high accuracy if the discharge coefficient is well characterized. The discharge coefficient C_d is determined for each TEA injector through a series of cold flow tests using water. Unfortunately, measuring the mass of TEA tank after the tests are not possible since the residue TEA must be evacuated from the tank right after the test for safety precautions. Consequently, TEA flow rates were calculated using theoretical methods. To validate this approach, five different injector tests were conducted with a known quantity of TEA. The average flow rate was determined by dividing the total TEA mass by the flow time obtained from both pressure data and the high-speed camera. This value was then compared with the value calculated from Eq. 3.1. The error between these two values fell within the range of ±3%, which is acceptable for validation.

Chapter 4:
RESULTS AND DISCUSSION

4.1 Ignition Delay and Boundary Determination Results

As previously mentioned, ignition delay and boundary determination tests were conducted for two distinct O/F ratios: 2.7 and 4.3, each under atmospheric conditions. The trends in ignition delay and boundaries are illustrated in Figure 4.1. Subsequently, the test results are summarized in Table 4.1. The area between the red dashed lines signifies the ignition boundary, indicating that the actual ignition boundary occurs at a certain angle within this zone.

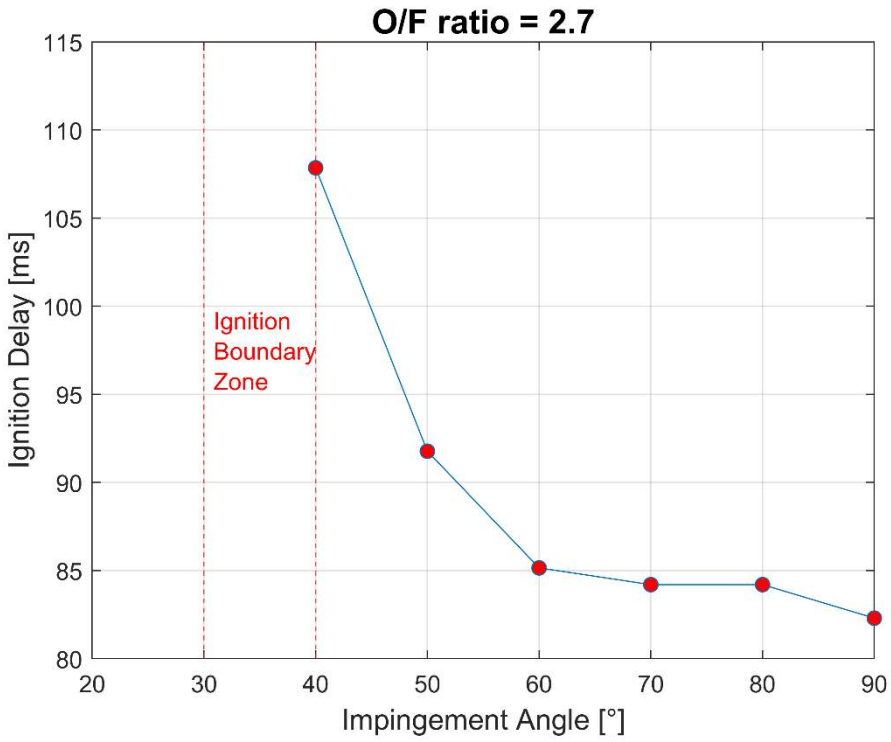

(a)

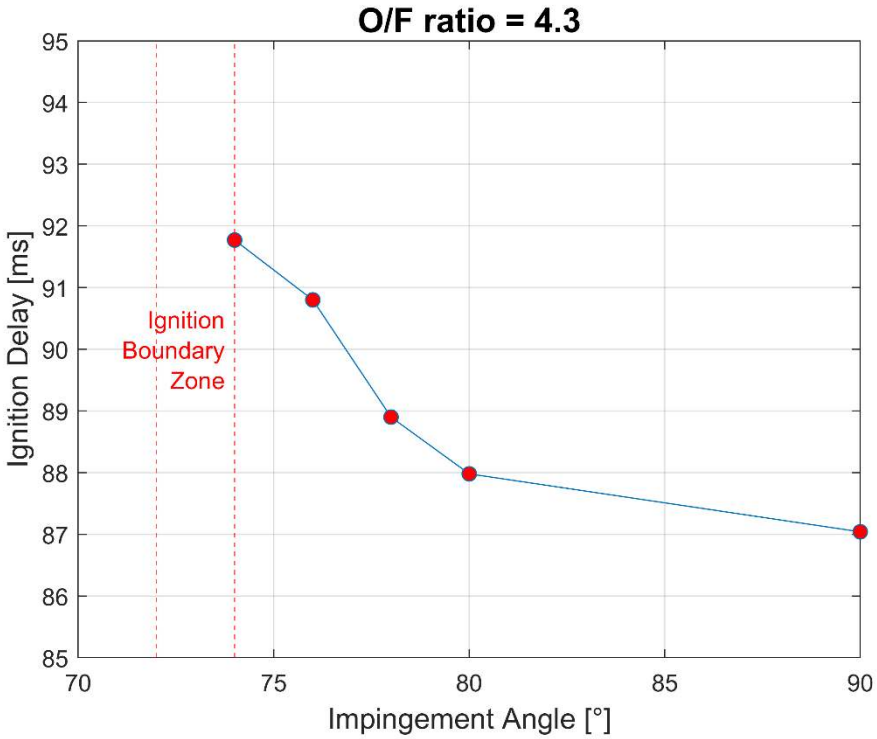

(b)

Figure 4.1: Variation of ignition delay times with respect to impingement angle for (a) O/F ratio of 2.7 and (b) O/F ratio of 4.3.

Table 4.1: Summary of test results.

O/F Ratio	Impingement Angle	Ignition Delay (ms)
2.64-2.76 (average 2.7)	90°	82.3
	80°	84.2
	70°	84.2
	60°	85.15
	50°	91.77
	40°	107.85
	30°	No ignition
4.21-4.35 (average 4.3)	90°	87.04
	80°	87.98
	78°	88.9
	76°	90.8
	74°	91.77
	72°	No ignition

For the O/F ratio of 2.7, no ignition occurred at the 30° angle, indicating that the ignition boundary lies between 30° and 40°. Between 90° and 60°, there's minimal variation in ignition delay times; however, below 60°, ignition delay times drastically increase. Ignition boundary values vary from 82.3 ms to 107.85 ms in general.

In the case of the O/F ratio of 4.3, no ignition occurred at 72°, setting the ignition boundary between 72° and 74°. Unlike the lower O/F ratio case, ignition delays show minor differences with respect to the impingement angle at this ratio. Ignition boundary values vary from 87.04 ms to 91.77 ms in general.

Overall, it can be inferred that ignition delay time rises as the impingement angle decreases. Moreover, with an increase in the O/F ratio, the ignition boundary shifts toward higher impingement angles, namely towards crossflow. Additionally, it's evident that ignition phenomena are more sensitive to impingement angle variations for higher O/F ratios compared to lower ones, given the narrower ignition delay range for O/F 4.3 compared to O/F 2.3. It is worth noting that, typically, the momentum ratio is employed instead of the O/F ratio when working with liquid-liquid bipropellant injectors. However, in this specific case, the calculated momentum ratios turned out to be equal to the calculated O/F ratios, given that the velocity of both TEA and N_2O jets is equal. Therefore, for the sake of simplicity and enhanced clarity, the O/F ratio was utilized in this study.

4.2 Mixed Spray Temperature Measurement Results

The temperature plots depicting the mixed spray are presented in Figure 4.2, where valve openings and closings are indicated. As previously illustrated in Figure 3.8, TC 1 was placed just downstream of the impingement point and TC 2 was set 15 mm downstream of TC 1. Additionally, TC 3 is placed 15 mm downstream of the TC 2 and close to the flame base. Unfortunately, due to a connector failure, no data was collected from TC 1, therefore only TC 2 and TC 3 are shown in Figure 4.2. The remaining TC’s operated without any problem.

Upon examination of Figure 4.2, the N_2O valve opens, and both TCs read almost identical values, indicating the presence of cold N_2O spray. Two seconds later, the TEA valve opens, followed by a warm-up period of 0.5 seconds for the mixed spray, eventually reaching its maximum value. TC 2, positioned near the impingement point, exhibits an

increase of approximately 30 K, while TC 3, closer to the flame base, experiences a significant rise of about 260 K. During ignition, TC 2 records an average temperature of 214 K, whereas TC 3 reads an average of 440 K. Subsequently, upon closure of both valves, temperatures swiftly drop and stabilize around 200-220 K until the N_2O feed line is completely evacuated. Overall, it's evident that no significant reaction occurs at or near the impingement point, with the ignition starting at a certain distance downstream. The sudden temperature increase upon TEA valve opening is likely attributed to radiative heat transfer from the flame.

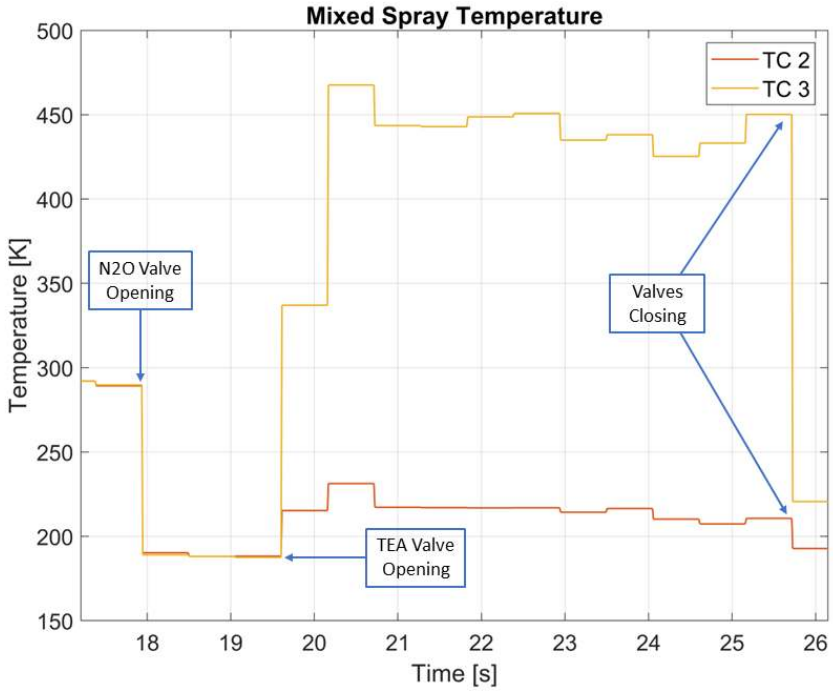

Figure 4.2: Mixed spray temperature measurements.

4.3 Discussion

4.3.1 Reactive Stream Separation

In the case of impinging hypergolic propellants, two distinct conditions exist: jet mixing and reactive stream separation (or blow apart), as illustrated in Figure 4.3. In the case of separation, a strong exothermic reaction occurs, usually very close to the impingement point, releasing enough heat for the streams to “blow apart” before mixing takes place. In this case, reaction rates are fast enough that the reaction interface

propagates downstream of the impingement point, preventing substantial spray mixing. However, if the reaction rates are slow, then sufficient mixing occurs for a uniform combustion. In this case, a mixing zone occurs through some distance downstream of the impingement point before ignition takes place.

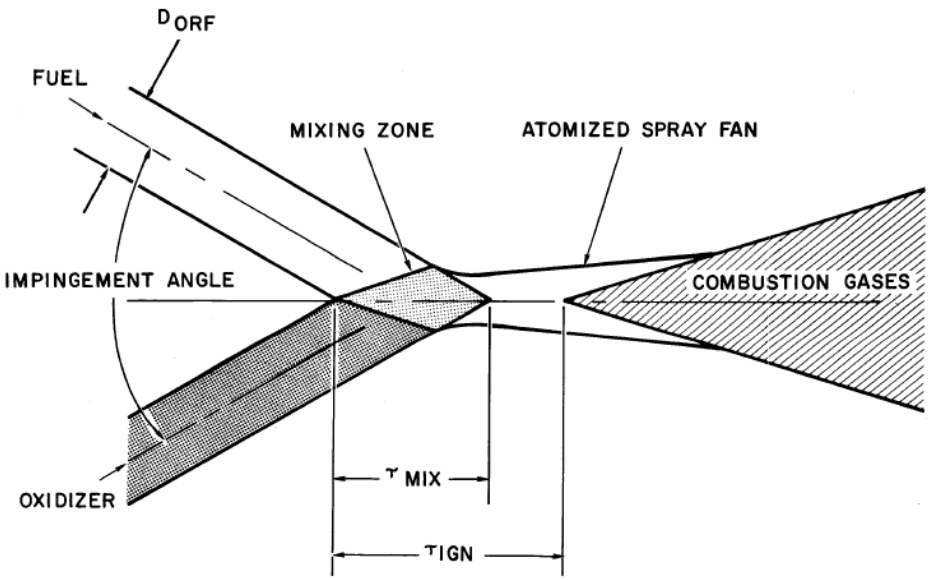

(a)

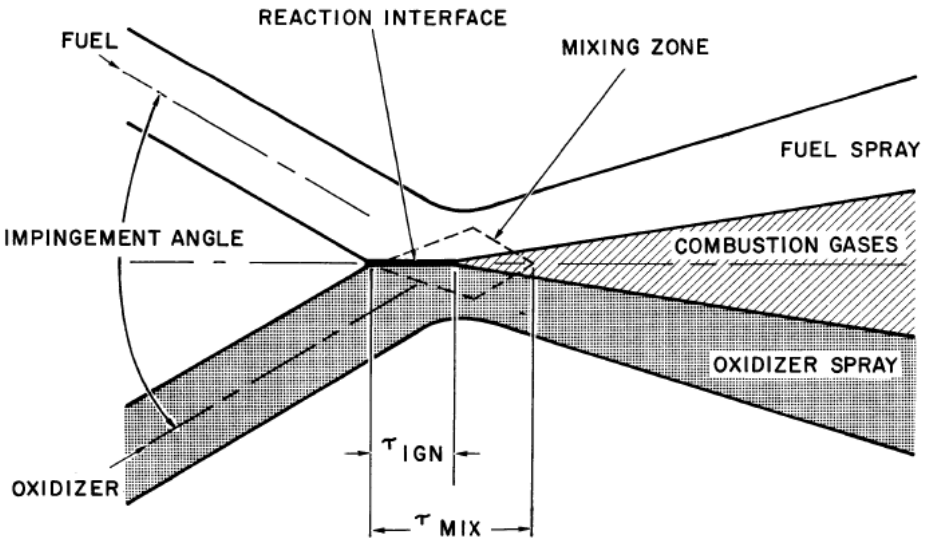

(b)

Figure 4.3: Impinging hypergolic streams in the case of (a) mixing and (b) separation (adapted from [48]).

In order to identify these two phenomena, two characteristic times are defined, τ_{ign} and τ_{mix}. τ_{ign} is the chemical reaction time necessary for the sufficient heat release so that ignition occurs, whereas τ_{mix} is the interfacial residence time of the streams within the mixing zone. When $\tau_{ign} < \tau_{mix}$, blow apart occurs while $\tau_{ign} > \tau_{mix}$, indicates mixing. The limit for separation can be defined at $\tau_{ign}=\tau_{mix}$. The relations for these two characteristic times are given in Eq. 4.1 and Eq. 4.2, taken from [49].

$$\tau_{ign} = \frac{1}{A} e^{E/RT} \tag{4.1}$$

$$\tau_{mix} = \frac{D}{V} \frac{1}{\sin(\theta/2)} \tag{4.2}$$

As can be seen, the chemical reaction time τ_{ign} exhibits an exponential correlation with temperature. Simultaneously, the mixing time τ_{mix} is a function of stream dimensions and influenced by factors including impingement angle θ, orifice diameter D, and jet velocity V. Consequently, the boundary for separation dynamically shifts in accordance with the ratio of orifice diameter to jet velocity D/V.

The investigation of the reactive stream separation phenomenon has revealed significant findings. In one experimental study [48], it was observed that blow apart instances increase with higher fluid temperatures and an increased ratio of D/V. Another research effort noted that separation occurs prominently for jet diameters larger than approximately 1 mm (0.04 inch), while diameters smaller than about 0.76 mm (0.03 inch) exhibit no separation [50]. Furthermore, this study highlighted that higher injection velocities correlate with reduced separation occurrence. In addition, it is stated that separation strength has a strong dependency on propellant combination as well.

Based on the aforementioned findings, it can be concluded that the tests conducted within the scope of this thesis likely do not exhibit separation phenomena. This assumption stems from the relatively small orifice diameters utilized (0.6 mm for TEA and 0.8 mm for N_2O) and the comparatively high jet velocities maintained (around 60 m/s for both streams), resulting in a relatively small D/V ratio.

4.3.2 Post-test Status of the Materials

As mentioned earlier, the combustion of TEA results in the formation of aluminum oxide (Al_2O_3), a persistent substance that adheres to contact surfaces, leading to potential clogging in feed systems and injectors. This scenario poses a disadvantage concerning the system's capability for multiple ignitions. Following each test, the accumulation of Al_2O_3 on instruments was assessed, with some instances depicted in Figure 4.4. Prolonged stay of Al_2O_3 within the fittings may cause them to be non-functional. For instance, after one test conducted for this study, the solenoid valve was left uncleaned for 24 hours, resulting in the complete adhesion of the valve contacts. Consequently, the valve failed to open.

Figure 4.4: Post-test Al_2O_3 accumulation.

Another significant issue arises from potential TEA leakage. Figure 4.5 showcases instances of TEA leaks impacting fittings, resulting in substantial damage to the threads. Even minor leaks or smokes can result in thread deformation due to Al_2O_3 accumulation, eventually leading to more severe leaks. Lessons learned from such occurrences is the necessity to consistently inspect fittings and instruments for any signs of deformation. Careful attention is required during the tightening of fittings, as insufficient tightening can lead directly to leaks, while excessive tightening may cause thread deformation, resulting in smoking or further leakage. Whenever feasible, welded joints can be a preferable solution.

Figure 4.5: Fitting deformation due to leakage.

Chapter 5:
CONCLUSION

This thesis investigates the ignition delay characteristics of triethylaluminum (TEA) combined with the oxidizing agent nitrous oxide (N_2O) for potential use as an ignition system. The experimental campaign includes two primary test phases: ignition delay and boundary determination, and mixed spray temperature measurement. In the first phase, ignition delay values were computed across various impingement angles at two distinct O/F ratios (2.7 and 4.3). The ignition boundary for each O/F ratio was established by gradually reducing the impingement angle until no ignition observed. Ignition delay values were calculated utilizing a high-speed camera. The second phase involved temperature measurements obtained from three different positions within the mixed spray, specifically the zone between the impingement point and the flame base. The test was conducted at a specific O/F ratio (2.7) and impingement angle (60°).

For the O/F ratio of 2.7, ignition boundary was found between 30° and 40°, with ignition delay values generally varying from 82.3 ms to 107.85 ms. Meanwhile, for the O/F ratio of 4.3, ignition boundary was found between 72° and 74°, with ignition delay values typically varying between 87.04 ms and 91.77 ms. Comparing the results between the two O/F ratios, minor differences in ignition delays were observed concerning the impingement angle at 4.3 ratio. The findings indicated that ignition delay time increases as the impingement angle decreases, and the ignition boundary shifts towards higher impingement angles with an increase in the O/F ratio. Notably, ignition phenomena were more sensitive to impingement angle variations for higher O/F ratios compared to lower ones, as evidenced by the narrower ignition delay range for O/F 4.3 in contrast to O/F 2.3.

Regarding temperature measurements, while the first thermocouple encountered a connector failure, the second and third thermocouples provided valuable data. Although the first thermocouple yielded no data due to this unfortunate incident, the remaining thermocouple data offered sufficient and useful information. Throughout ignition, the second thermocouple recorded an average temperature of 214 K, while the third reached 440 K. The results indicated that no significant reaction occurs at or near the impingement point, suggesting ignition initiation occurring at a certain distance downstream.

The research demonstrated an absence of reactive stream separation, a commonly observed phenomenon in impinging hypergolic jets, highlighting sufficient spray mixing. These findings offer valuable insights for the conceptual design of an igniter. For example, they underscore the importance of comprehensive investigations into ignition delay times and boundaries before beginning with the conceptual design of an igniter. Additionally, it should be noted that higher O/F ratios introduce more strict constraints on operable impingement angle ranges, necessitating careful consideration in conceptual designs.

Future work will expand the studies on ignition delay and boundary determination across additional O/F ratios. In addition, efforts will be dedicated to resolving component deformations caused by aluminum oxide (Al_2O_3) formation to enable a multi-ignition-capable system design. Finally, a focus will be placed on creating a conceptual design for a pyrophoric ignition system. The designed ignition system will ultimately be applied for igniting a hybrid rocket motor intended for use in space applications.

BIBLIOGRAPHY

[1] C. D. Brown, *Elements of Spacecraft Design*, American Institute of Aeronautics and Astronautics, Inc., 2002.

[2] G. P. Sutton and O. Biblarz, *Rocket Propulsion Elements*, New York: John Wiley & Sons, Inc., 2001.

[3] B. M. Nufer, "A summary of NASA and USAF hypergolic propellant related spills and fires," NASA, Florida, NASA/TP-2009-214769, 2009.

[4] S. A. Whitmore, Z. W. Peterson and S. D. Eilers, "Deep throttle of a nitrous oxide and Hhydroxyl-terminated polybutadiene hybrid rocket motor," *Journal of Propulsion and Power,* vol. 30, no. 1, pp. 78-86, 2014.

[5] S. A. Whitmore, Z. W. Peterson and S. D. Eilers, "Closed-loop precision throttling of a hybrid rocket motor," *Journal of Propulsion and Power,* vol. 30, no. 2, pp. 325-336, 2014.

[6] B. Cantwell, A. Karabeyoglu and D. Altman, "Recent advances in hybrid propulsion," *International Journal of Energetic Materials and Chemical Propulsion,* vol. 9, no. 4, pp. 305-326, 2010.

[7] A. Karabeyoglu, E. Toson and B. Evans, ""O/F Shift" in hybrid rockets"," in *50th AIAA/ASME/SAE/ASEE Joint Propulsion Conference*, Cleveland, Ohio, 2014.

[8] G. Story, "Large-scale hybrid motor testing," in *Fundamentals of Hybrid Rocket Combustion and Propulsion*, American Institute of Aeronautics and Astronautics, 2007, p. 513-552.

[9] G. Frenken, E. Vermeulen, F. Bouquet and B. Sanders, "Development status of the ignition system for Vinci," in *38th AIAA/ASME/SAE/ASEE Joint Propulsion Conference & Exhibit*, Indianapolis, IN, 2002.

[10] Boeing, *Space Shuttle Main Engine Orientation*, [Online]. (1998). Accessed: May 2023. Available: http://large.stanford.edu/courses/2011/ph240/nguyen1/docs/SSME_PRESENTATION.pdf

[11] D. H. Huang and D. K. Huzel, *Modern Engineering for Design of Liquid-Propellant Rocket Engines*, American Institute of Aeronautics and Astronautics, Inc., Whasington, DC, 1992.

[12] D. H. Barret, "Solid rocket motor igniters," NASA, Cleveland, OH, SP-8051, 1971.

[13] A. Okninski, P. Surmacz, B. Bartkowiak, T. Mayer, K. Sobczak, M. Pakosz, D. Kaniewski, J. Matyszewski, G. Rarata and P. Wolanski, "Development of green storable hybrid rocket propulsion technology using 98% hydrogen peroxide as oxidizer," *Aerospace,* vol. 8, no. 9, p. 234, 2021.

[14] B. Ahn, H. Kang, E. Lee, Y. Yun and S. Kwon, "Design of multiport grain with hydrogen peroxide hybrid rocket," *Journal of Propulsion and Power,* vol. 34, no. 5, pp. 1189-1197, 2018.

[15] M. D. Wilson, "Catalytic decomposition of nitrous oxide monopropellant for hybrid motor ignition", MS Thesis, Utah State University, Logan, UT, USA, 2013.

[16] Q. Paquot, "Storable green oxidizers for hybrid rocket propulsion", MS Thesis, Politechnico di Milano, Milano, Italy, 2021.

[17] L. S. Jacobsen, C. D. Carter, T. A. Jackson, S. Williams, J. Barnett, D. Bivolaru and S. Kuo, "Plasma-assisted ignition in scramjets," *Journal of Propulsion and Energy,* vol. 24, no. 4, pp. 641-654, 2008.

[18] I. Nakagawa, "Plasma torch igniter for hybrid rockets," *Science and Technology of Energetic Materials,* vol. 80, no. 2, pp. 54-60, 2019.

[19] Rocketdyne, "Advanced ignition systems final report," North American Rockwell Corporation, Canoga Park CA, USA, CR-119928, 1971.

[20] L. C. Liou, "Combustion-wave ignition for rocket engines," in *JANNAF Propulsion Meeting*, Indianapolis, IN, USA, 1992.

[21] P. Lungu, C. Bauer and O. J. Haidn, "Design aspects and characterisation of a resonance igniter for oxygen/methane in-orbit propulsion systems," in *8th European Conference for Aeronautics and Space Sciences (EUCASS)*, Madrid, Spain, 2019.

[22] C. Bauer, P. Lungu and O. J. Haidn, "Numerical investigation of a resonance ignition sytem," in *8th European Conference for Aeronautics and Space Sciences (EUCASS)*, Madrid, Spain, 2019.

[23] A. Young, *The Saturn V F-1 Engine: Powering Apollo Into Space*, New York: Springer Science & Business Media, 2008.

[24] SpaceX, *Falcon User's Guide*, (2021). Accessed: May 2023. [Online]. Available: https://www.spacex.com/media/falcon-users-guide-2021-09.pdf

[25] R. J. Kniffen, B. McKinney and P. Estey, "Hybrid rocket development at the american rocket company," in *AIAA/SAE/ASME/ASEE 26th Joint Propulsion Conference*, Orlando, FL, USA 1990.

[26] R. J. Kniffen, "Development status of the 200,000 lbf thrust hybrid rocket booster," in *AIAA Space Programs and Technologies Conference*, Huntsville, AL, USA, 1992.

[27] K. J. Flittie, P. N. Estey and R. J. Kniffen, "The aquila launch vehicle: a hybrid propulsion space booster," *Acta Astronautica,* vol. 28, pp. 99-110, 1992.

[28] J. S. McFarlane, R. J. Kniffen and J. Lichatowich, "Design and testing of amroc's 250,000 pound thrust hybrid motor," in *AIAA/SAE/ASME/ASEE 29th Joint Propulsion Conference and Exhibit*, Monterey, CA, USA, 1993.

[29] M. D. Jones, T. M. Abel and D. J. Weeks, "Subscale hybrid rocket motor testing at the marshall space flight center in support of the hybrid propulsion demonstration program," in *33rd Joint Propulsion Conference and Exhibit*, Seattle, WA, USA, 1997.

[30] T. A. Boardman, R. L. Carpenter and S. E. Claflin, "A comparative study of the effects of liquid- versus gaseous-oxygen injection on combustion stability in 11-inch-diameter hybrid motors," in *33rd Joint Propulsion Conference and Exhibit*, Seattle, WA, USA, 1997.

[31] T. A. Boardman, T. M. Abel, S. E. Claflin and C. W. Schaeffer, "Design and test planning for a 250-klbf-thrust hybrid rocket motor under the hybrid propulsion demonstration program," in *33rd Joint Propulsion Conference and Exhibit*, Seattle, WA, USA, 1997.

[32] M. D. Bradford, R. J. Kniffen and B. C. McKinney, "Hybrid Rocket Combustion Enhancement". U.S. Patent 5,582,001, Dec. 10, 1996.

[33] T. W. Ryan, S. T. Schwab and W. W. Harlowe, "Ignition delays, heats of combustion, and reaction rates of aluminum alkyl derivatives used as ignition and combustion enhancers for supersonic combustion," NASA, Hampton, VA, NASA-CR-189581, 1992.

[34] J. D. Desain, M. J. Degges and B. B. Brady, "Pyrophoric ignition system testing for in-space bi-propellant propulsion systems," Aerospace Corporation, 2018.

[35] *Triethylaluminum, 93%,* [Print]; abcr: Karlsruhe, Germany, 2020.

[36] *Triethylaluminum*, [Print]; Merck: Taufkirchen, Germany, 2021.

[37] D. B. Malpass, "Commercially available metal alkyls and their use in polyolefin catalysts," in *Handbook of Transition Metal Polymerization Catalysts*, John Wiley & Sons, Inc., 2010, pp. 1-28.

[38] *TEAL: Triethylaluminum*, [Online]; Nouryon: Sep. 17, 2021. Available: https://www.nouryon.com/globalassets/inriver/resources/pds-teal-polymer-production-glo-en.pdf. (accessed May 2023).

[39] Trelleborg. *Materials Chemical Compatibility Guide*, (2012). Accessed: May 2023. [Online]. Available: https://www.trelleborg.com/-/media/tss-media-repository/tss_website/pdf-and-other-literature/brochures/mat_chem_comp_gb_en.pdf?revision=5ab08743-3efa-4245-a951-ac5960c5290e

[40] C. L. Filtration. *Chemical Compatibility Guide*, (2000). Accessed: May 2023. [Online]. Available: https://clearlakefiltration.com/chemical-compatibility-chart.pdf

[41] I. Graco. *Chemical Compatibility Guide*, (2013). Accessed: May 2023. [Online]. Available: https://www.graco.com/content/dam/graco/ipd/literature/misc/chemical-compatibility-guide/Graco_ChemCompGuideEN-B.pdf

[42] M. B. Smith, "Monomer-dimer equilibria of liquid aluminum alkyls. I. Triethylaluminum," *The Journal of Physical Chemistry,* vol. 71, no. 2, pp. 364-370, 1967.

[43] *NIST Chemistry Webbook, SRD 69, Aluminum, triethyl-*, National Institute of Standards and Technology, 2023. [Online]. Available: https://webbook.nist.gov/cgi/inchi?ID=C97938&Mask=2#Thermo-Condensed

[44] J. P. Leal ve J. A. M. Simoes, "Standard Enthalpy of Formation of Triethylaluminum," *Organometallics,* vol 12, pp. 1442-1444, 1993.

[45] NOAA. *Triethylaluminum,* (1999). May 2023. [Online]. Available: https://cameochemicals.noaa.gov/chris/TAL.pdf

[46] *NIST Chemistry WebBook, SRD 69, Nitrous Oxide*, National Institute of Standards and Technology, 2023. [Online]. Available: https://webbook.nist.gov/cgi/cbook.cgi?ID=C10024972&Mask=1#Thermo-Gas

[47] H. W. Douglass and W. H. Nurick, "Liquid rocket engine injectors," NASA, Cleveland, OH, SP-8089, 1976.

[48] B. R. Lawver ve B. P. Breen, "Hypergolic stream impingement phenomena - nitrogen tetroxide/hydrazine," NASA, Cleveland, OH , CR-72444, 1968.

[49] B. P. Breen, L. B. Zung, B. R. Lawver, T. C. Kosvic and D. E. Coats, "Injection and combustion of hypergolic propellants," Air Force Rocket Propulsion Laboratory, Edwards, CA, AFRPL-TR-69-48, 1969.

[50] W. H. Nurick ve J. D. Cordill, "Reactive Stream Seperation Photography-Final Report," NASA, Canoga Park, CA, CR-119246, 1971.